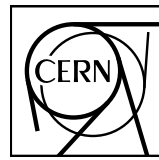


EUROPEAN ORGANIZATION FOR NUCLEAR RESEARCH



CERN-EP-2023-187
28 August 2023

Skewness and kurtosis of mean transverse momentum fluctuations at the LHC energies

ALICE Collaboration*

Abstract

The first measurements of skewness and kurtosis of mean transverse momentum ($\langle p_T \rangle$) fluctuations are reported in Pb–Pb collisions at $\sqrt{s_{NN}} = 5.02$ TeV, Xe–Xe collisions at $\sqrt{s_{NN}} = 5.44$ TeV and pp collisions at $\sqrt{s} = 5.02$ TeV using the ALICE detector. The measurements are carried out as a function of system size $\langle dN_{\text{ch}}/d\eta \rangle_{|\eta|<0.5}^{1/3}$, using charged particles with transverse momentum (p_T) and pseudorapidity (η), in the range $0.2 < p_T < 3.0$ GeV/ c and $|\eta| < 0.8$, respectively. In Pb–Pb and Xe–Xe collisions, positive skewness is observed in the fluctuations of $\langle p_T \rangle$ for all centralities, which is significantly larger than what would be expected in the scenario of independent particle emission. This positive skewness is considered a crucial consequence of the hydrodynamic evolution of the hot and dense nuclear matter created in heavy-ion collisions. Furthermore, similar observations of positive skewness for minimum bias pp collisions are also reported here. Kurtosis of $\langle p_T \rangle$ fluctuations is found to be in good agreement with the kurtosis of Gaussian distribution, for most central Pb–Pb collisions. Hydrodynamic model calculations with MUSIC using Monte Carlo Glauber initial conditions are able to explain the measurements of both skewness and kurtosis qualitatively from semicentral to central collisions in Pb–Pb system. Color reconnection mechanism in PYTHIA8 model seems to play a pivotal role in capturing the qualitative behavior of the same measurements in pp collisions.

© 2023 CERN for the benefit of the ALICE Collaboration.

Reproduction of this article or parts of it is allowed as specified in the CC-BY-4.0 license.

*See Appendix A for the list of collaboration members

1 Introduction

The properties of the hot and dense nuclear matter created in heavy-ion collisions at relativistic energies can be studied using event-by-event fluctuations of different quantities like multiplicity, net-charge, mean transverse momentum ($\langle p_T \rangle$), etc. [1–4]. The analysis of event-by-event fluctuations of these variables offers valuable means to probe the dynamical fluctuations that originate from the production of a quark-gluon plasma (QGP) [5] phase during heavy-ion collisions. Fluctuations in the thermodynamic quantity of temperature, which are associated with the phase transition in the quantum chromodynamics (QCD) phase diagram, can manifest themselves in the fluctuations of the $\langle p_T \rangle$ of the final-state particles [6]. A non-monotonic behavior of $\langle p_T \rangle$ fluctuations as a function of centrality or incident energy was suggested as one of the possible signals of the QGP [3]. However, $\langle p_T \rangle$ fluctuations are also affected by non-thermodynamic variations in the initial geometry of the collision that include fluctuations in the initial size, shape and orientation of the colliding nuclei, and the fluctuating number of nucleons participating in the collision. The $\langle p_T \rangle$ fluctuations measured at RHIC did not show any beam energy dependence, and the non-monotonic behavior with centrality was also not observed [7]. The previous measurements of $\langle p_T \rangle$ fluctuations in Pb–Pb collisions at centre-of-mass energy per nucleon pair, $\sqrt{s_{\text{NN}}} = 2.76$ TeV in ALICE [8] suggested a connection of the observed fluctuations of the $\langle p_T \rangle$ to the fluctuations in the initial state of the collision. Qualitatively, the data obtained from model calculations using the string melting approach in A Multi-Phase Transport (AMPT) model [9], where partons rescatter and recombine through a hadronic coalescence scheme, exhibit agreement with the observed results [8]. The string melting version was introduced in the model [10] to address and account for the effects of flow originating from the entire partonic system in the overlap volume of heavy-ion collisions, as opposed to considering only the contributions from minijet partons in the default version. By incorporating the string melting approach, the model was able to simulate the collective behavior of the partonic system during the early stages of the collision, leading to a more accurate description of the experimental observations of elliptic flow. The $\langle p_T \rangle$ fluctuations were also calculated in the color glass condensate (CGC) [11, 12] formulation, where they have been related to initial spatial fluctuations of glasma flux tube via their coupling to a collective flow field. The comparison of these calculations with data showed a good agreement in the semicentral and central collisions [13].

The space-time evolution of the QGP phase produced in the relativistic heavy-ion collisions is well described by the relativistic viscous hydrodynamics [14–16]. In Ref. [17], it has been proposed that the skewness of $\langle p_T \rangle$ fluctuations can serve as an essential probe of the hydrodynamic behavior of the system created in heavy-ion collisions. The $\langle p_T \rangle$ of the particles emitted at freeze-out was found to be correlated to the initial energy of the system at the beginning of the hydrodynamic evolution, instead of the energy of the system at freeze-out [18]. The fluctuations of $\langle p_T \rangle$ are therefore found to be related to the fluctuations of initial energy density in an *effective* hydrodynamic description [19]. It was shown that the skewness of $\langle p_T \rangle$ fluctuations are driven by the skewness of the initial energy density fluctuations, which implies that the $\langle p_T \rangle$ fluctuations arise from the same collective dynamics in the QGP phase that give rise to anisotropic flow. Furthermore, employing initial conditions from the TRENTo model [20] and evolving them with the V-USPHYDRO viscous hydrodynamic [21] simulations predicted positive skewness of $\langle p_T \rangle$ fluctuations surpassing expectations in independent particle emission scenarios. Additional information regarding these simulations can be found in Ref. [17].

The fluctuations in $\langle p_T \rangle$ of charged particles can be influenced by various physical effects, such as collective behavior of the system formed in the collisions, fluctuations in the number of participating nucleons, or the presence of jets and resonance decays. Examining the higher-order terms of $\langle p_T \rangle$ fluctuations will enable us to delve deeper into the intricate mechanisms underlying the observed fluctuations and acquire valuable insights. In this article, the first experimental study of skewness and kurtosis of $\langle p_T \rangle$ fluctuations that represent the third- and fourth-order fluctuations of $\langle p_T \rangle$ are reported at the Large Hadron Collider (LHC) energies. The observables used in this analysis are introduced in Sec. 2. Here, the multiparticle

p_T correlators used to study the $\langle p_T \rangle$ fluctuations are defined. A brief description of the subsystems of ALICE detector relevant to this analysis is given in Sec. 3. The analysis technique and the method of estimating statistical and systematic uncertainties for the measurements are explained in Sec. 4. The skewness and the kurtosis of $\langle p_T \rangle$ fluctuations as a function of system size and the interpretation of results using theoretical models are presented in Sec. 5. The major findings of the analysis are summarized in Sec. 6.

2 Observables

In this analysis, the fluctuations in event-by-event $\langle p_T \rangle$ of charged particles are investigated using multiparticle p_T correlators. The event-by-event $\langle p_T \rangle$ is defined as

$$\langle p_T \rangle = \frac{\sum_{i=1}^{N_{\text{ch}}} p_{T,i}}{N_{\text{ch}}}, \quad (1)$$

where $p_{T,i}$ is the transverse momentum of the i th particle and N_{ch} is the total number of charged particles in the event. Alternatively, one can employ the standard moment method for event-by-event analysis of $\langle p_T \rangle$ fluctuations. The moment method calculates various order moments of the $\langle p_T \rangle$ distribution, providing a comprehensive evaluation of the total fluctuation accounting for both the statistical and dynamical (non-statistical) parts. The advantage of employing multiparticle p_T correlators [22, 23] is that they yield zero values for events with randomly sampled particles, thereby effectively isolating the non-statistical fluctuations of interest. The expressions for the two-particle p_T correlator ($\langle \Delta p_{T,i} \Delta p_{T,j} \rangle$) and three-particle p_T correlator ($\langle \Delta p_{T,i} \Delta p_{T,j} \Delta p_{T,k} \rangle$) [17] are denoted by Eqs. 3 and 4, respectively, where Q_n is defined as

$$Q_n = \sum_{i=1}^{N_{\text{ch}}} p_{T,i}^n. \quad (2)$$

Constraints on the indices in summations in the definition of correlators ensure that self-correlations are eliminated. The algebraic expressions of the correlators in terms of Q_n 's where $n = 1, 2, \dots$ were derived to account for the practical limitations of calculating multiparticle p_T correlators with nested loops, especially when dealing with events characterized by large multiplicities. Since, the values of Q_n can be obtained with Eq. 2 employing a single loop, it becomes feasible to directly utilize the later expressions with Q_n s in Eqs. 3 and 4 for the calculation of two- and three-particle p_T correlators, respectively. On similar lines, the four-particle p_T correlator ($\langle \Delta p_{T,i} \Delta p_{T,j} \Delta p_{T,k} \Delta p_{T,l} \rangle$) is derived as shown in Eq. 5. These two-, three-, and four-particle correlators are related to the variance, skewness, and kurtosis of the $\langle p_T \rangle$ distribution, respectively.

$$\langle \Delta p_{T,i} \Delta p_{T,j} \rangle = \left\langle \frac{\sum_{\substack{i,j \\ i \neq j}}^{N_{\text{ch}}} (p_{T,i} - \langle \langle p_T \rangle \rangle)(p_{T,j} - \langle \langle p_T \rangle \rangle)}{N_{\text{ch}}(N_{\text{ch}} - 1)} \right\rangle_{\text{ev}} = \left\langle \frac{Q_1^2 - Q_2}{N_{\text{ch}}(N_{\text{ch}} - 1)} \right\rangle_{\text{ev}} - \left\langle \frac{Q_1}{N_{\text{ch}}} \right\rangle_{\text{ev}}^2, \quad (3)$$

$$\begin{aligned} \langle \Delta p_{T,i} \Delta p_{T,j} \Delta p_{T,k} \rangle &= \left\langle \frac{\sum_{\substack{i,j,k \\ i \neq j \neq k}}^{N_{\text{ch}}} (p_{T,i} - \langle \langle p_T \rangle \rangle)(p_{T,j} - \langle \langle p_T \rangle \rangle)(p_{T,k} - \langle \langle p_T \rangle \rangle)}{N_{\text{ch}}(N_{\text{ch}} - 1)(N_{\text{ch}} - 2)} \right\rangle_{\text{ev}} \\ &= \left\langle \frac{Q_1^3 - 3Q_2Q_1 + 2Q_3}{N_{\text{ch}}(N_{\text{ch}} - 1)(N_{\text{ch}} - 2)} \right\rangle_{\text{ev}} - 3 \left\langle \frac{Q_1^2 - Q_2}{N_{\text{ch}}(N_{\text{ch}} - 1)} \right\rangle_{\text{ev}} \left\langle \frac{Q_1}{N_{\text{ch}}} \right\rangle_{\text{ev}} + 2 \left\langle \frac{Q_1}{N_{\text{ch}}} \right\rangle_{\text{ev}}^3, \end{aligned} \quad (4)$$

$$\begin{aligned}
\langle \Delta p_{T,i} \Delta p_{T,j} \Delta p_{T,k} \Delta p_{T,l} \rangle &= \left\langle \frac{\sum_{i,j,k,l}^{N_{ch}} (p_{T,i} - \langle \langle p_T \rangle \rangle)(p_{T,j} - \langle \langle p_T \rangle \rangle)(p_{T,k} - \langle \langle p_T \rangle \rangle)(p_{T,l} - \langle \langle p_T \rangle \rangle)}{N_{ch}(N_{ch}-1)(N_{ch}-2)(N_{ch}-3)} \right\rangle_{ev} \\
&= \left\langle \frac{Q_1^4 - 6Q_4 + 8Q_1Q_3 - 6Q_1^2Q_2 + 3Q_2^2}{N_{ch}(N_{ch}-1)(N_{ch}-2)(N_{ch}-3)} \right\rangle_{ev} \\
&\quad - 4 \left\langle \frac{Q_1^3 - 3Q_2Q_1 + 2Q_3}{N_{ch}(N_{ch}-1)(N_{ch}-2)} \right\rangle_{ev} \left\langle \frac{Q_1}{N_{ch}} \right\rangle_{ev} \\
&\quad + 6 \left\langle \frac{Q_1^2 - Q_2}{N_{ch}(N_{ch}-1)} \right\rangle_{ev} \left\langle \frac{Q_1}{N_{ch}} \right\rangle_{ev}^2 - 3 \left\langle \frac{Q_1}{N_{ch}} \right\rangle_{ev}^4. \tag{5}
\end{aligned}$$

In the above equations, angular brackets $\langle \dots \rangle_{ev}$ denote an average over all events and $\langle \langle p_T \rangle \rangle = \langle Q_1/N_{ch} \rangle_{ev}$ is the event-by-event $\langle p_T \rangle$ averaged over all events. The standardized skewness ($\gamma_{\langle p_T \rangle}$) and the intensive skewness ($\Gamma_{\langle p_T \rangle}$) are two measures of the skewness of the $\langle p_T \rangle$ distribution, constructed using the two-particle and three-particle p_T correlators [17], given by

$$\gamma_{\langle p_T \rangle} = \frac{\langle \Delta p_{T,i} \Delta p_{T,j} \Delta p_{T,k} \rangle}{\langle \Delta p_{T,i} \Delta p_{T,j} \rangle^{3/2}}, \tag{6}$$

and

$$\Gamma_{\langle p_T \rangle} = \frac{\langle \Delta p_{T,i} \Delta p_{T,j} \Delta p_{T,k} \rangle \langle \langle p_T \rangle \rangle}{\langle \Delta p_{T,i} \Delta p_{T,j} \rangle^2}. \tag{7}$$

The kurtosis $\kappa_{\langle p_T \rangle}$ of $\langle p_T \rangle$ distribution is defined as

$$\kappa_{\langle p_T \rangle} = \frac{\langle \Delta p_{T,i} \Delta p_{T,j} \Delta p_{T,k} \Delta p_{T,l} \rangle}{\langle \Delta p_{T,i} \Delta p_{T,j} \rangle^2}. \tag{8}$$

The article focuses on analyzing higher order fluctuations of $\langle p_T \rangle$, particularly the third and fourth order. Three key observables, namely the standardized skewness, intensive skewness, and kurtosis of the $\langle p_T \rangle$ distribution (defined in Eqs. 6, 7, and 8, respectively), are investigated as a function of the system size in Pb–Pb collisions at $\sqrt{s_{NN}} = 5.02$ TeV, Xe–Xe collisions at $\sqrt{s_{NN}} = 5.44$ TeV, and pp collisions at $\sqrt{s} = 5.02$ TeV.

3 Experimental setup

The measurements reported in the article are obtained using the data recorded by the ALICE detector at the LHC. A detailed description of the ALICE detector and its performance can be found in Refs. [24, 25]. The primary sub-detectors relevant to this analysis are the Time Projection Chamber (TPC) [26], the Inner Tracking System (ITS) [25], and the V0 detector [27]. The TPC and ITS are used for tracking and reconstructing the primary vertex, while the V0 detector is used for triggering and the default centrality estimation. The V0 detector consists of two scintillator arrays, V0A and V0C, located on both sides of the interaction point, covering the pseudorapidity (η) intervals $2.8 < \eta < 5.1$ and $-3.7 < \eta < -1.7$, respectively [27]. The data analyzed here are obtained from Pb–Pb collisions at $\sqrt{s_{NN}} = 5.02$ TeV, Xe–Xe collisions at $\sqrt{s_{NN}} = 5.44$ TeV, and pp collisions at $\sqrt{s} = 5.02$ TeV. These datasets were recorded in 2015 (pp and Pb–Pb) and 2017 (Xe–Xe) during LHC Run 2. A minimum bias (MB) trigger condition is applied to select collision events that requires at least one hit in both the V0A and the V0C detectors. Events that pass the MB trigger criteria and have a reconstructed primary vertex position within 10 cm along the beam axis to the nominal interaction point are selected in the analysis. Using information from multiple detectors as described in Ref. [25], events with more than one reconstructed primary interaction

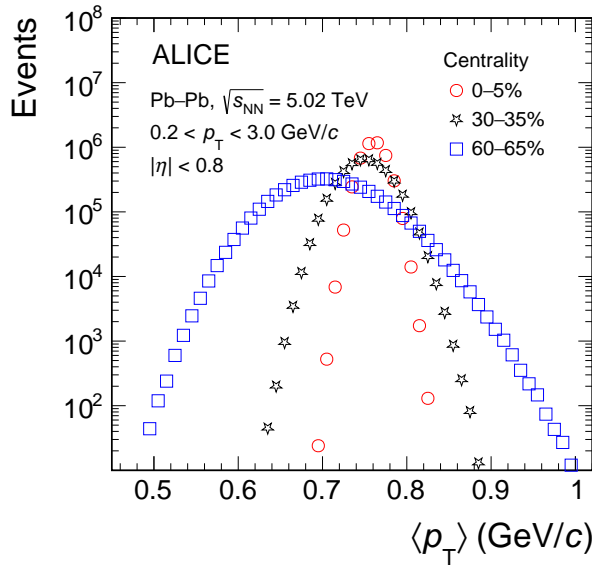


Figure 1: Efficiency uncorrected mean transverse momentum distributions for different centrality classes in Pb–Pb collisions at $\sqrt{s_{\text{NN}}} = 5.02$ TeV.

vertex (pile-up events) are rejected. In total, 84 million Pb–Pb collisions, 1.2 million Xe–Xe collisions, and 95 million pp collisions pass the above mentioned criteria and are used for the analysis.

The charged-particle tracks reconstructed using the ITS and the TPC in the ALICE central barrel are selected in the kinematic range $0.2 < p_T < 3.0$ GeV/c and $|\eta| < 0.8$, where p_T is the track momentum in the plane transverse to the beam axis. The accepted tracks exhibit approximately uniform azimuthal acceptance in this region. The tracks that have at least 70 out of a maximum possible 159 reconstructed space points in the TPC, and at least one hit in the two innermost layers of the ITS (ITS has in total six layers) are selected. This selection assures a resolution better than $300 \mu\text{m}$ [25] on the distance-of-closest-approach (DCA) to the primary vertex in the plane perpendicular (DCA_{xy}) and parallel (DCA_z) to the beam axis for the selected tracks. In order to suppress the contamination from secondary particles, the DCA of the tracks to the primary vertex must be within 1 cm in the longitudinal direction and 0.1 cm in the transverse plane. Moreover, the χ^2 per degree of freedom of the track fit to the space points in the TPC and the ITS are required to be less than 4 (2.5 for Pb–Pb) and 36, respectively.

4 Data analysis

The mean transverse momentum $\langle p_T \rangle$ distributions obtained for three different centrality classes in Pb–Pb collisions at $\sqrt{s_{\text{NN}}} = 5.02$ TeV are shown in Fig. 1. The distributions are not corrected for detector inefficiencies. The centrality classes are formed by splitting the events based on the measured amplitude distribution in the V0A and V0C detectors as described in Refs. [28, 29]. The mean of the $\langle p_T \rangle$ distributions are found to increase whereas the width of the distribution decreases from peripheral to central collisions. The larger width of the distribution for peripheral (lower multiplicity) collisions indicates larger fluctuations compared to the central (higher multiplicity) collisions. Similar behavior is observed in Xe–Xe collisions at $\sqrt{s_{\text{NN}}} = 5.44$ TeV and pp collisions at $\sqrt{s} = 5.02$ TeV.

Before starting the analysis with the $\langle p_T \rangle$ correlators presented in Sec. 2, it is important to demonstrate that these fluctuations are not a trivial consequence of fluctuating N_{ch} in a given centrality class. The definition of $\langle p_T \rangle$ in Eq. 1 clearly shows that the varying multiplicity in different events of the same centrality class can affect the $\langle p_T \rangle$ distributions and consequently its fluctuations. To examine whether

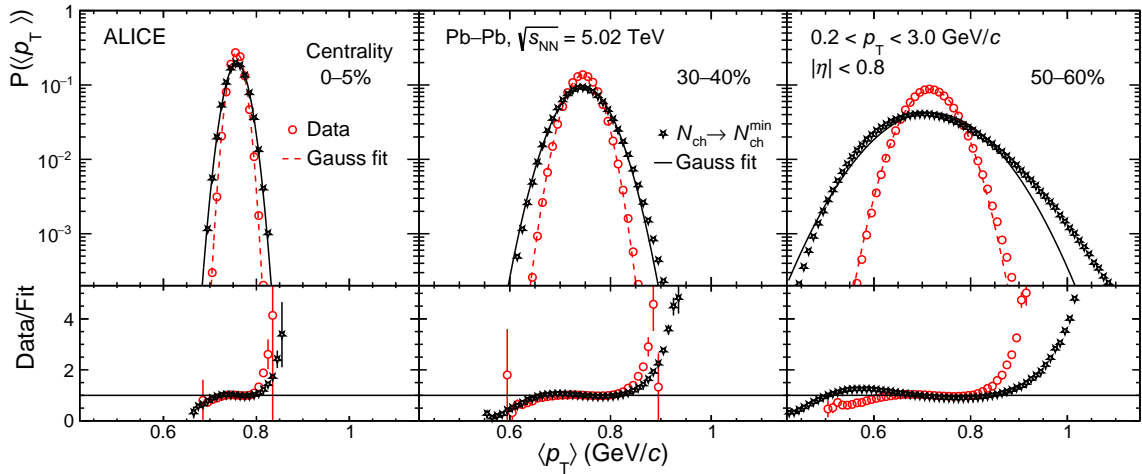


Figure 2: Comparison of event-by-event mean transverse momentum $\langle p_T \rangle$ distribution from actual analysis and modified analysis in which N_{ch} in each event is fixed to N_{ch}^{\min} (N_{ch}^{\min} is the minimum number of charged particles in a given centrality class) and N_{ch}^{\min} number of particles are selected in each event randomly for the 0–5% (left), 30–40% (middle), and 50–60% (right) centrality classes.

these fluctuations persist after removing the stochastic effects of the multiplicity, a check is performed. For each centrality class, the minimum number of tracks per event in the kinematic acceptance of the analysis, N_{ch}^{\min} is determined. In each event of the centrality class, the N_{ch}^{\min} number of tracks are then selected randomly to calculate the genuine $\langle p_T \rangle$ distribution free from biases of multiplicity fluctuations. The left panel of Fig. 2 shows the $\langle p_T \rangle$ distribution for the 0–5% central events in Pb–Pb collisions at $\sqrt{s_{NN}} = 5.02$ TeV. The distribution in red markers shows the original event-by-event $\langle p_T \rangle$ distribution in which N_{ch} fluctuates whereas the distribution shown with black markers is the $\langle p_T \rangle$ distribution in which N_{ch} is fixed to N_{ch}^{\min} in each event of the centrality class. A Gaussian function is used to fit the two distributions and the ratio of data to fit is shown in the bottom panel of Fig. 2. The ratio shows that the data points are above the fit in the right-side of the distribution, and below the fit in the left-side, indicating that the $\langle p_T \rangle$ distributions are positively skewed. The $\langle p_T \rangle$ distributions exhibit substantial deviations from a Gaussian distribution even under the condition of a fixed N_{ch} , thereby reflecting the analogous traits observed in the original distribution with fluctuating N_{ch} . The middle and right panels of Fig. 2 visually exemplify the consistent manifestation of these characteristics within the distributions of $\langle p_T \rangle$ for both semicentral and peripheral collisions. It is concluded that the positive skewness in the event-by-event $\langle p_T \rangle$ distributions is not a trivial consequence of event-by-event statistical fluctuations of N_{ch} , and therefore new and non-trivial information can be extracted from higher-order moments of $\langle p_T \rangle$ fluctuations.

The $\langle p_T \rangle$ correlators described in Eqs. 3, 4, and 5 are calculated using charged-particle tracks in different centrality (multiplicity) classes. For Pb–Pb collisions, the observables are analyzed in 18 equal-width centrality classes ranging between zero to ninety percent, i.e., 0–5%, 5–10%, ..., 85–90%. For Xe–Xe collisions, the total number of events are divided into four centrality classes, 0–20%, 20–40%, 40–60%, and 60–80%. The centrality classes are taken wider for Xe–Xe collisions because of the limited data sample. In pp collisions, the events are classified into ten multiplicity classes, 0–1%, 1–5%, 5–10%, 10–15%, 15–20%, 20–30%, 30–40%, 40–50%, 50–70%, and 70–100%. The method of defining these multiplicity classes can be found in Ref. [30].

The $\langle p_T \rangle$ correlators are calculated in the unit multiplicity bins of a given centrality class, and then merged using centrality bin width correction formula [31]. In this way, both the effects of multiplicity fluctuations, and the necessity of using non-trivial multiplicity weight to determine all-event averages

Table 1: Contributions to the total systematic uncertainty on standardized skewness $\gamma_{\langle p_T \rangle}$, intensive skewness $\Gamma_{\langle p_T \rangle}$, and kurtosis $\kappa_{\langle p_T \rangle}$ in Pb–Pb collisions at $\sqrt{s_{NN}} = 5.02$ TeV, Xe–Xe collisions at $\sqrt{s_{NN}} = 5.44$ TeV, and pp collisions at $\sqrt{s} = 5.02$ TeV. Ranges are given where the uncertainties depend on centrality or multiplicity.

Observables	Sources of systematic uncertainty	Pb–Pb	Xe–Xe	pp
$\gamma_{\langle p_T \rangle}$	Vertex z -position	0.7–2.7%	1.5–9.1%	0.3–0.8%
	Pileup	0.5–6.4%	–	–
	$\chi^2_{\text{TPC}}/n_{\text{TPCclusters}}$	0.5–2.6%	3.4–6.5%	0.1–0.4%
	$\chi^2_{\text{ITS}}/n_{\text{ITSclusters}}$	0.5–2.2%	3.6–11.3%	< 0.1%
	$n_{\text{TPCcrossedrows}}$	0.6–3.8%	2.6–6.8%	0.9–1.9%
	DCA _{xy}	0.6–4.5%	2.5–7.3%	0.5–1.1%
	DCA _z	0.4–1.8%	2.8–5.9%	< 0.1%
	MC closure	2.3%	2.6%	2.7%
	Total	2.9–8.7%	9.1–17.2%	2.9–3.6%
$\Gamma_{\langle p_T \rangle}$	Vertex z -position	0.6–2.7%	1.7–9.1%	0.3–0.8%
	Pileup	0.5–6.3%	–	–
	$\chi^2_{\text{TPC}}/n_{\text{TPCclusters}}$	0.4–2.7%	3.6–6.9%	0.1–0.3%
	$\chi^2_{\text{ITS}}/n_{\text{ITSclusters}}$	0.4–2.2%	3.7–11.4%	< 0.1%
	$n_{\text{TPCcrossedrows}}$	0.8–3.8%	3.0–7.0%	0.3–1.7%
	DCA _{xy}	0.7–4.7%	0.4–4.2%	0.3–1%
	DCA _z	0.4–1.9%	2.7–6.0%	< 0.1%
	MC closure	3.6%	2.3%	0.4%
	Total	4–9%	9.5–17.6%	0.8–2.1%
$\kappa_{\langle p_T \rangle}$	Vertex z -position	0.1–3.6%	0.9–4.5%	0.1–1.4%
	Pileup	0.2–4.5%	–	–
	$\chi^2_{\text{TPC}}/n_{\text{TPCclusters}}$	0.1–1.8%	0.9–4.6%	0.1–1.1%
	$\chi^2_{\text{ITS}}/n_{\text{ITSclusters}}$	0.1–0.9%	1.2–3.9%	< 0.1%
	$n_{\text{TPCcrossedrows}}$	0.1–1.3%	3.0–7.0%	0.3–1.7%
	DCA _{xy}	0.1–2.3%	0.3–0.9%	0.5–3.3%
	DCA _z	0.1–2.9%	0.7–1.9%	< 0.1%
	MC closure	0.3%	1.3%	0.9%
	Total	0.5–7.3%	2.7–11.7% %	1.8–4.7%

from single-event averages, are eliminated. The statistical uncertainties are evaluated using the bootstrap method. By repeatedly resampling the dataset and analyzing each resample, the bootstrap method provides a robust and computationally feasible approach for estimating the uncertainties associated with the observed results. It allows for a comprehensive assessment of the variability in the data, taking into account the inherent fluctuations and dependencies present in the measurements. The systematic uncertainties on the observables are estimated separately for each collision system by varying event and track selection criteria. The uncertainties related to the event selection include the variation of the accepted vertex position along the beam direction and pileup cut where applicable. The uncertainties due to track selection include the variation of the selection criteria on DCA_{xy} , DCA_z , the number of reconstructed space points in the TPC, and the quality of the track fit from their nominal values. Systematic uncertainties obtained from the contribution of each of these sources are considered as uncorrelated and the total systematic uncertainty on the observables is obtained by adding them in quadrature. Table 1 shows the summary of the contributions to the total systematic uncertainty on standardized skewness, intensive skewness, and kurtosis in Pb–Pb, Xe–Xe, and pp collisions.

The standardized skewness, intensive skewness, and kurtosis reported in this draft are considered robust and independent of detection efficiencies [17]. The detector inefficiencies cancel to leading order within these ratios, despite their potential presence in individual p_T correlators. Consequently, efficiency correction is not carried out for these ratios. The robustness of the measured ratios is further affirmed by performing a Monte Carlo (MC) closure test. The MC closure test uses simulations based on different event generators for producing particles that corresponds to generated (true) results and GEANT3 [32] for the transport of particles through the geometry of ALICE detectors. For Pb–Pb and Xe–Xe collisions, the MC events are generated using HIJING (Heavy-Ion Jet Interaction Generator) [33] whereas for pp collisions, the events are produced by PYTHIA8 [34, 35] event generator with Monash2013 tune. The experimental conditions prevailing during the data taking are accounted for in the generated events using GEANT3 by reproducing the actual configuration of different detectors during the runs. Results obtained from the generated events are compared with their corresponding reconstructed ones (without applying efficiency corrections), and they show a good agreement within uncertainties. The ratio of the reconstructed to the generated results for the observables are fitted with zeroth-order polynomial functions to quantify the amount of closure obtained. The percentages of agreement for standardized skewness, intensive skewness, and kurtosis are 97.3%, 99.6% and 99.1%, respectively, in pp collisions at $\sqrt{s} = 5.02$ TeV. Similar study is also performed for the other two collision systems, Pb–Pb collisions at $\sqrt{s_{NN}} = 5.02$ and Xe–Xe collisions at $\sqrt{s_{NN}} = 5.44$ TeV. The percentages of closure for the observables (standardized skewness, intensive skewness, kurtosis) in Pb–Pb (Xe–Xe) collisions are found to be 97.7% (97.4%), 96.4% (97.7%), and 99.7% (98.7%). These differences are added to the systematic uncertainties and reported in Table 1.

To study how the skewness and kurtosis of $\langle p_T \rangle$ distributions vary with the size of the collision system and to have a comparison between heavy-ion collisions (Pb–Pb and Xe–Xe) and small systems like pp collisions, expressing the centrality (multiplicity for pp collisions) classes as average charged particle multiplicity density ($\langle dN_{ch}/d\eta \rangle_{|\eta|<0.5}$) is more suitable. The conversion of centrality to $\langle dN_{ch}/d\eta \rangle_{|\eta|<0.5}$ is performed using the measured values of $\langle dN_{ch}/d\eta \rangle_{|\eta|<0.5}$ for certain centrality classes from Ref. [36] for Pb–Pb collisions. It should be noted that the centrality classes used in this analysis are narrower and different from that in the reference. A linear relation is observed between average number of charged particles ($\langle N_{acc} \rangle$) in the kinematic range ($|\eta| < 0.8$ and $0.2 < p_T < 0.3$ GeV/c) of this analysis and $\langle dN_{ch}/d\eta \rangle_{|\eta|<0.5}$ over the full centrality range. The extracted fit parameters from the linear relation between $\langle N_{acc} \rangle$ and $\langle dN_{ch}/d\eta \rangle_{|\eta|<0.5}$ were used to assign a value of $\langle dN_{ch}/d\eta \rangle_{|\eta|<0.5}$ for any value of $\langle N_{acc} \rangle$. Hence, by calculating the $\langle N_{acc} \rangle$ for the centrality classes of this analysis, the corresponding value of $\langle dN_{ch}/d\eta \rangle_{|\eta|<0.5}$ is obtained. This method was previously used in the study of second-order fluctuations of $\langle p_T \rangle$ in Ref. [8]. Similar approach is followed for Xe–Xe collisions using $\langle dN_{ch}/d\eta \rangle_{|\eta|<0.5}$ values of centrality classes from Ref. [37]. For pp collisions, the measured values of $\langle dN_{ch}/d\eta \rangle_{|\eta|<0.5}$

are taken from Ref. [30] since the multiplicity classes are the same.

5 Results

5.1 Standardized skewness

The standardized skewness of charged particles produced in Pb–Pb collisions at $\sqrt{s_{\text{NN}}} = 5.02$ TeV and Xe–Xe collisions at $\sqrt{s_{\text{NN}}} = 5.44$ TeV as a function of system size denoted by the cubic root of average charged particle multiplicity density, $\langle dN_{\text{ch}}/d\eta \rangle_{|\eta|<0.5}^{1/3}$ is shown in Fig. 3. The femtoscopic radii associated with the radius of the fireball at freeze-out, scale linearly with $\langle dN_{\text{ch}}/d\eta \rangle_{|\eta|<0.5}^{1/3}$ and therefore it is used as a proxy for the system size [38]. The uncertainties on $\langle dN_{\text{ch}}/d\eta \rangle_{|\eta|<0.5}^{1/3}$ are obtained by propagating the uncertainty on $\langle dN_{\text{ch}}/d\eta \rangle_{|\eta|<0.5}$. It is observed that $\gamma_{\langle p_T \rangle}$ decreases with increasing $\langle dN_{\text{ch}}/d\eta \rangle_{|\eta|<0.5}^{1/3}$ for both Pb–Pb and Xe–Xe collisions. This is generally expected from fluctuations in a dilution scenario caused by superposition of partially independent particle-emitting sources [7, 8]. If the fluctuations in $\langle p_T \rangle$ have been purely statistical and generated by finite multiplicity (N), then $\gamma_{\langle p_T \rangle}$ would have a dependence of $1/\sqrt{N}$. A slight enhancement of $\gamma_{\langle p_T \rangle}$ in the most central ($\langle dN_{\text{ch}}/d\eta \rangle_{|\eta|<0.5}^{1/3} > 11$) Pb–Pb collisions is also observed within uncertainty. One of the probable reasons could be the reduction of two-particle correlations $\langle \Delta p_i \Delta p_j \rangle$ towards the central collisions reported previously in Ref. [8]. Hydrodynamic model calculations from Ref. [17] that uses T_RENTo initial conditions evolved by hydrodynamic code v-USPHYDRO referred as v-USPHYDRO model in the figures are compared with the data for both Pb–Pb and Xe–Xe collisions. A small specific shear viscosity, $\eta/s = 0.047$ is used in the v-USPHYDRO model. As shown in Fig. 3, the v-USPHYDRO model calculations capture the general system size dependence of the measurement, but fail to describe it quantitatively. In the model, $\gamma_{\langle p_T \rangle}$ is larger in Pb–Pb collisions compared to Xe–Xe collisions for almost all multiplicities, however data do not show such system dependence. Model calculations using HIJING [33], which incorporates various phenomena like multiple minijet production with initial and final state radiation or nuclear effects such as parton shadowing and jet quenching, are shown in the figure. HIJING considers nucleus–nucleus collisions as superposition of independent binary collisions of wounded nucleons. The latest version of the model, HIJING/ $B\bar{B}$ v2.0 with shadowing and jet quenching effects [39] is used. The $\gamma_{\langle p_T \rangle}$ in HIJING model exhibits a strong dependence with $\langle dN_{\text{ch}}/d\eta \rangle_{|\eta|<0.5}^{1/3}$ and reproduces the measurement in the semiperipheral to semicentral region. Calculations performed using the MC-Glauber+MUSIC model, which adopts the Glauber Monte Carlo [40] approach to generate initial conditions for the collisions, followed by the MUSIC hydrodynamic model [41] with $\eta/s = 0.1$ are presented. Notably, both the HIJING and MC-Glauber+MUSIC model utilize the Monte Carlo Glauber initial conditions, with the primary difference lying in the subsequent evolution. While HIJING lacks the implementation of collective phenomena, MUSIC incorporates such effects. Interestingly, the results obtained for the $\gamma_{\langle p_T \rangle}$ in Pb–Pb collisions remain same for both models from semiperipheral to semicentral collisions. This prompts the question of whether the $\gamma_{\langle p_T \rangle}$ is primarily sensitive to the details of the initial conditions.

The results in Pb–Pb and Xe–Xe are also compared with the measurements carried out in pp collisions at $\sqrt{s} = 5.02$ TeV. The $\gamma_{\langle p_T \rangle}$ in pp collisions shows a steeper decrease with increasing $\langle dN_{\text{ch}}/d\eta \rangle_{|\eta|<0.5}^{1/3}$ compared to heavy-ion collisions. The observed $\gamma_{\langle p_T \rangle}$ is also found smaller in pp collisions than in Pb–Pb collisions in the overlapping $\langle dN_{\text{ch}}/d\eta \rangle_{|\eta|<0.5}^{1/3}$ region. The measurements in pp collisions are compared with PYTHIA8 [35] model, which is a pQCD based MC event generator. The PYTHIA8 model is found to describe numerous experimental results in pp collisions at LHC energies quite successfully [42–44]. This model can involve color reconnection (CR) mechanism [45] in pp collisions, which could contribute to explaining certain collective effects that have been observed in these collisions. Comparison of the measurements in pp collisions with PYTHIA8 model for both cases, with and without enabling CR mechanism (referred as PYTHIA8 CR ON and PYTHIA8 CR OFF), are presented. PYTHIA8 CR OFF

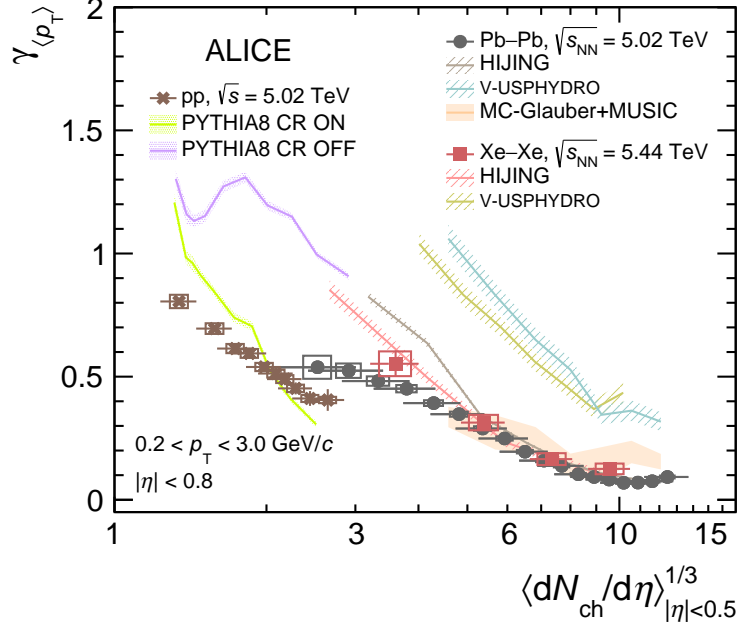


Figure 3: Standardized skewness $\gamma_{\langle p_T \rangle}$ shown as a function of $\langle dN_{ch}/d\eta \rangle_{|\eta|<0.5}^{1/3}$ in Pb–Pb collisions at $\sqrt{s_{NN}} = 5.02$ TeV, Xe–Xe collisions at $\sqrt{s_{NN}} = 5.44$ TeV, and pp collisions at $\sqrt{s} = 5.02$ TeV. The predictions from different event generators and hydrodynamic model calculations from v-USPHYDRO [17] and MC-Glauber+MUSIC [40, 41] are denoted by colored bands. The statistical (systematic) uncertainties are represented by vertical bars (boxes).

model calculations utterly fail to describe the measurements both qualitatively and quantitatively. On the other hand, PYTHIA CR ON calculations reproduce the dependence of $\gamma_{\langle p_T \rangle}$ with $\langle dN_{ch}/d\eta \rangle_{|\eta|<0.5}^{1/3}$ although with a larger slope.

5.2 Intensive skewness

Figure 4 shows the intensive skewness studied with respect to $\langle dN_{ch}/d\eta \rangle_{|\eta|<0.5}^{1/3}$ in Pb–Pb collisions at $\sqrt{s_{NN}} = 5.02$ TeV and Xe–Xe collisions at $\sqrt{s_{NN}} = 5.44$ TeV. The colored dashed lines indicate the independent baselines $\Gamma_{independent}$ evaluated for each system separately. The formula [17] used to calculate the independent baseline for intensive skewness is

$$\Gamma_{independent} = \frac{\langle (p_T - \langle p_T \rangle)^3 \rangle \langle p_T \rangle}{\langle (p_T - \langle p_T \rangle)^2 \rangle^2} , \quad (9)$$

where $\langle p_T \rangle$ is the average transverse momentum in given centrality class. The p_T spectra for different centrality classes are the input distributions for the calculation of $\Gamma_{independent}$ as a function of centrality. The second and third central moments of the p_T distributions, $\langle (p_T - \langle p_T \rangle)^2 \rangle$ and $\langle (p_T - \langle p_T \rangle)^3 \rangle$ are evaluated using the p_T spectrum for each centrality class and the ratio of these moments gives the $\Gamma_{independent}$ for that centrality class. For Pb–Pb and Xe–Xe collisions, the p_T spectra are taken from Refs. [46] and [47], respectively. Consecutively, the centralities are converted into $\langle dN_{ch}/d\eta \rangle_{|\eta|<0.5}$ and $\langle dN_{ch}/d\eta \rangle_{|\eta|<0.5}^{1/3}$. A positive intensive skewness, larger than the independent baseline, is observed in both Pb–Pb and Xe–Xe collisions as a function of system size. This observation is in accordance with the predictions from the v-USPHYDRO hydrodynamic model calculations. The v-USPHYDRO model results describe the data qualitatively but do not show quantitative agreement. The HIJING model calculations though seem to capture the decreasing trend of the measurements in the semiperipheral to semicentral region ($3.8 \leq \langle dN_{ch}/d\eta \rangle_{|\eta|<0.5}^{1/3} \leq 8.9$) but are unable to explain the rise of $\Gamma_{\langle p_T \rangle}$ in the measurements

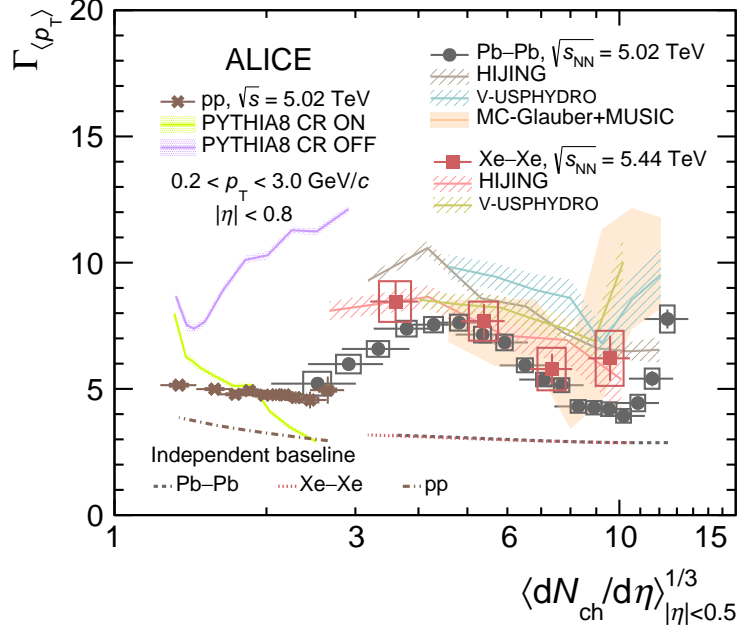


Figure 4: Intensive skewness $\Gamma_{\langle p_T \rangle}$ shown as a function of $\langle dN_{ch}/d\eta \rangle_{|\eta|<0.5}^{1/3}$ in Pb–Pb collisions at $\sqrt{s_{NN}} = 5.02$ TeV, Xe–Xe collisions at $\sqrt{s_{NN}} = 5.44$ TeV, and pp collisions at $\sqrt{s} = 5.02$ TeV. The colored dashed lines represent the independent baseline for each system. The predictions from different event generators and hydrodynamic model calculations from v-USPHYDRO [17] and MC-Glauber+MUSIC [40, 41] are denoted by colored bands. The statistical (systematic) uncertainties are represented by vertical bars (boxes).

from the semicentral to central region ($9.0 \leq \langle dN_{ch}/d\eta \rangle_{|\eta|<0.5}^{1/3} \leq 12.4$). The observed increase in both $\gamma_{\langle p_T \rangle}$ and $\Gamma_{\langle p_T \rangle}$ for $\langle dN_{ch}/d\eta \rangle_{|\eta|<0.5}^{1/3} > 11$ in Pb–Pb collisions might be indicative of the onset of thermalization [48, 49]. This phenomenon is distinct from hydrodynamization, which could occur in smaller systems and at shorter timescales. As a direct consequence of thermalization, a significant increase of the skewness of $\langle p_T \rangle$ fluctuations is predicted for most central collisions. If the system thermalizes, $\langle p_T \rangle$ increases with density which is a characteristic phenomenon in relativistic fluid dynamics. At fixed multiplicity, larger density corresponds to smaller volume and correspondingly larger impact parameter which suggests that the rise of skewness results from a reduction in impact parameter fluctuations within the most central collisions. The MC-Glauber+MUSIC model calculations exhibit similar behavior observed in the measurements of $\Gamma_{\langle p_T \rangle}$ in Pb–Pb collisions and provide better agreement quantitatively than the v-USPHYDRO model results. The increase of $\Gamma_{\langle p_T \rangle}$ for central collisions in the measurements, seems to be depicted by both of the hydrodynamic model calculations with different initial conditions and therefore demands theoretical inputs to understand this rise.

The measurement performed in pp collisions at $\sqrt{s} = 5.02$ TeV is also shown along with its independent baseline. For pp collisions, the baseline is calculated using the p_T spectra from Ref. [50]. The hydrodynamic prediction of positive intensive skewness above of its baseline is pronounced in the measurements in pp collisions as well. The distinct non-monotonic behavior observed in Pb–Pb collisions as a function of $\langle dN_{ch}/d\eta \rangle_{|\eta|<0.5}^{1/3}$ is noticeably attenuated in pp collisions. The $\Gamma_{\langle p_T \rangle}$ exhibits a subtle, monotonic decrease as $\langle dN_{ch}/d\eta \rangle_{|\eta|<0.5}^{1/3}$ increases in pp collisions. In the PYTHIA8 CR OFF model, the results for $\Gamma_{\langle p_T \rangle}$ exhibit an increase as $\langle dN_{ch}/d\eta \rangle_{|\eta|<0.5}^{1/3}$ increases, which is in direct contrast to the observations from the PYTHIA8 CR ON model. While the PYTHIA8 CR ON model appears to be in closer agreement with the experimental measurements compared to CR OFF, neither model adequately captures the qualitative behavior observed in the measurements.

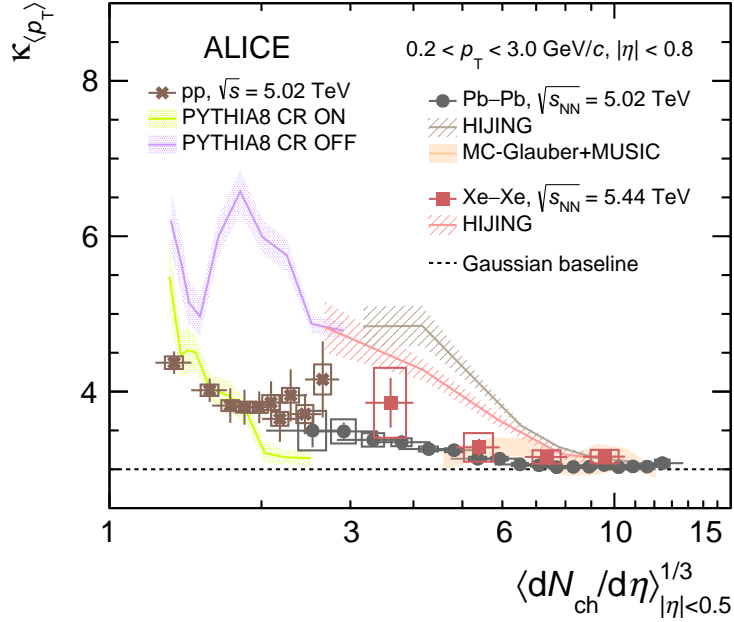


Figure 5: Kurtosis $\kappa_{\langle p_T \rangle}$ shown as a function of $\langle dN_{ch}/d\eta \rangle_{|\eta|<0.5}^{1/3}$ in Pb–Pb collisions at $\sqrt{s_{NN}} = 5.02$ TeV, Xe–Xe collisions at $\sqrt{s_{NN}} = 5.44$ TeV and pp collisions at $\sqrt{s} = 5.02$ TeV. The predictions from different event generators and hydrodynamic calculations from MC-Glauber+MUSIC model [40, 41] are represented by colored bands. The dashed line indicates the Gaussian baseline. The statistical (systematic) uncertainties are represented by vertical bars (boxes).

5.3 Kurtosis

The kurtosis evaluated using Eq. 5 as a function of $\langle dN_{ch}/d\eta \rangle_{|\eta|<0.5}^{1/3}$ in Pb–Pb collisions at $\sqrt{s_{NN}} = 5.02$ TeV and Xe–Xe collisions at $\sqrt{s_{NN}} = 5.44$ TeV is shown in Fig. 5. The $\kappa_{\langle p_T \rangle}$ for a Gaussian distribution, which serves as a baseline for independent particle production, is shown with dotted line. The $\kappa_{\langle p_T \rangle}$ is found to decrease with increasing system size in Pb–Pb and Xe–Xe collisions and approaches the Gaussian baseline towards the most central Pb–Pb collisions. The measurements are compared with HIJING model calculations for both Pb–Pb and Xe–Xe collisions. While the HIJING model successfully capture the decreasing trend observed in the measurements with respect to $\langle dN_{ch}/d\eta \rangle_{|\eta|<0.5}^{1/3}$, it exhibits a pronounced and rapid decrease in $\kappa_{\langle p_T \rangle}$ compared to the data points. This is related to trivial system size dependence of $\kappa_{\langle p_T \rangle}$ in HIJING that should follow $1/N$ dependence. Throughout the entire range of $\langle dN_{ch}/d\eta \rangle_{|\eta|<0.5}^{1/3}$, the HIJING model overestimates the measurements. The MC-Glauber+MUSIC calculations reproduce the measurements in the central to midperipheral region ($5.4 \leq \langle dN_{ch}/d\eta \rangle_{|\eta|<0.5}^{1/3} \leq 12.4$). The measurements in pp collisions at $\sqrt{s} = 5.02$ TeV are also shown in the Fig. 5. In pp collisions, the $\kappa_{\langle p_T \rangle}$ decreases with $\langle dN_{ch}/d\eta \rangle_{|\eta|<0.5}^{1/3}$ and remains consistently above the Gaussian baseline even for the highest value of $\langle dN_{ch}/d\eta \rangle_{|\eta|<0.5}^{1/3}$. Calculations of $\kappa_{\langle p_T \rangle}$ in PYTHIA8 show similar behavior with $\langle dN_{ch}/d\eta \rangle_{|\eta|<0.5}^{1/3}$ as in data when CR mechanism is turned ON. PYTHIA8 CR OFF model completely fails to describe the measured $\kappa_{\langle p_T \rangle}$.

6 Summary

In summary, first results on higher order fluctuations of mean transverse momentum ($\langle p_T \rangle$) of charged particles, skewness, and kurtosis in Pb–Pb, Xe–Xe, and pp collisions at LHC energies are presented.

Two measures of skewness, standardized skewness and intensive skewness, are studied using three- and two-particle p_T correlators as a function of system size ($\langle dN_{ch}/d\eta \rangle_{|\eta|<0.5}^{1/3}$). The standardized skewness is found to decrease with increasing system size in all three collision systems. Positive intensive skewness, larger than the baseline and consistent with the predictions from the hydrodynamics studies in Ref. [17], is observed in both Pb–Pb and Xe–Xe collisions. The anticipated positive intensive skewness for A–A collisions is likewise confirmed in pp collisions at similar collision energy. HIJING model calculations, which do not incorporate hydrodynamic evolution, are able to exhibit the qualitative behavior of intensive skewness in the region of $3.8 \leq \langle dN_{ch}/d\eta \rangle_{|\eta|<0.5}^{1/3} \leq 8.9$. The striking rise of intensive skewness in the most central region is unexplained by HIJING. This effect is, however captured in the hydrodynamic calculations of both v-USPHYDRO and MC-Glauber+MUSIC models. The MC-Glauber+MUSIC model shows good agreement with the measurements of the standardized skewness and intensive skewness in the region of $4.8 \leq \langle dN_{ch}/d\eta \rangle_{|\eta|<0.5}^{1/3} \leq 12.4$. In contrast, the v-USPHYDRO model, which utilizes TRRENTo initial conditions, overestimates both measures of skewness. The discrepancy between the results obtained from the two hydrodynamic models suggests that these measurements can provide valuable insights into the initial stages of the collision. Also, the standardized skewness in HIJING and MC-Glauber+MUSIC models exhibits similar behavior, suggesting that its sensitivity may primarily be attributed to the details of the initial conditions rather than the subsequent evolution. In pp collisions, the PYTHIA8 model with the color reconnection mechanism enabled is able to qualitatively reproduce the measurements. The kurtosis measured using the two- and four-particle p_T correlators shows a decrease with the system size. This decreasing behavior is reproduced by the HIJING model calculations in Pb–Pb and Xe–Xe collisions, which, however, do not show a quantitative agreement with the measurements. Hydrodynamic calculations from MC-Glauber+MUSIC model explain the measurement well in the region of $4.8 \leq \langle dN_{ch}/d\eta \rangle_{|\eta|<0.5}^{1/3} \leq 12.4$. The value of kurtosis from the MC-Glauber+MUSIC model has a similar value to that from a Gaussian distribution. The measurements of kurtosis in Pb–Pb collisions also agreeing with the Gaussian baseline for highest values of the system size, hint about the production of a locally thermalized system in most central Pb–Pb collisions.

Acknowledgements

The ALICE Collaboration would like to thank all its engineers and technicians for their invaluable contributions to the construction of the experiment and the CERN accelerator teams for the outstanding performance of the LHC complex. The ALICE Collaboration gratefully acknowledges the resources and support provided by all Grid centres and the Worldwide LHC Computing Grid (WLCG) collaboration. The ALICE Collaboration acknowledges the following funding agencies for their support in building and running the ALICE detector: A. I. Alikhanyan National Science Laboratory (Yerevan Physics Institute) Foundation (ANSL), State Committee of Science and World Federation of Scientists (WFS), Armenia; Austrian Academy of Sciences, Austrian Science Fund (FWF): [M 2467-N36] and Nationalstiftung für Forschung, Technologie und Entwicklung, Austria; Ministry of Communications and High Technologies, National Nuclear Research Center, Azerbaijan; Conselho Nacional de Desenvolvimento Científico e Tecnológico (CNPq), Financiadora de Estudos e Projetos (Finep), Fundação de Amparo à Pesquisa do Estado de São Paulo (FAPESP) and Universidade Federal do Rio Grande do Sul (UFRGS), Brazil; Bulgarian Ministry of Education and Science, within the National Roadmap for Research Infrastructures 2020-2027 (object CERN), Bulgaria; Ministry of Education of China (MOEC) , Ministry of Science & Technology of China (MSTC) and National Natural Science Foundation of China (NSFC), China; Ministry of Science and Education and Croatian Science Foundation, Croatia; Centro de Aplicaciones Tecnológicas y Desarrollo Nuclear (CEADEN), Cubaenergía, Cuba; Ministry of Education, Youth and Sports of the Czech Republic, Czech Republic; The Danish Council for Independent Research | Natural Sciences, the VILLUM FONDEN and Danish National Research Foundation (DNRF), Denmark; Helsinki Institute of Physics (HIP), Finland; Commissariat à l’Energie Atomique (CEA) and

Institut National de Physique Nucléaire et de Physique des Particules (IN2P3) and Centre National de la Recherche Scientifique (CNRS), France; Bundesministerium für Bildung und Forschung (BMBF) and GSI Helmholtzzentrum für Schwerionenforschung GmbH, Germany; General Secretariat for Research and Technology, Ministry of Education, Research and Religions, Greece; National Research, Development and Innovation Office, Hungary; Department of Atomic Energy Government of India (DAE), Department of Science and Technology, Government of India (DST), University Grants Commission, Government of India (UGC) and Council of Scientific and Industrial Research (CSIR), India; National Research and Innovation Agency - BRIN, Indonesia; Istituto Nazionale di Fisica Nucleare (INFN), Italy; Japanese Ministry of Education, Culture, Sports, Science and Technology (MEXT) and Japan Society for the Promotion of Science (JSPS) KAKENHI, Japan; Consejo Nacional de Ciencia (CONACYT) y Tecnología, through Fondo de Cooperación Internacional en Ciencia y Tecnología (FONCICYT) and Dirección General de Asuntos del Personal Académico (DGAPA), Mexico; Nederlandse Organisatie voor Wetenschappelijk Onderzoek (NWO), Netherlands; The Research Council of Norway, Norway; Commission on Science and Technology for Sustainable Development in the South (COMSATS), Pakistan; Pontificia Universidad Católica del Perú, Peru; Ministry of Education and Science, National Science Centre and WUT ID-UB, Poland; Korea Institute of Science and Technology Information and National Research Foundation of Korea (NRF), Republic of Korea; Ministry of Education and Scientific Research, Institute of Atomic Physics, Ministry of Research and Innovation and Institute of Atomic Physics and Universitatea Națională de Știință și Tehnologie Politehnica București, Romania; Ministry of Education, Science, Research and Sport of the Slovak Republic, Slovakia; National Research Foundation of South Africa, South Africa; Swedish Research Council (VR) and Knut & Alice Wallenberg Foundation (KAW), Sweden; European Organization for Nuclear Research, Switzerland; Suranaree University of Technology (SUT), National Science and Technology Development Agency (NSTDA) and National Science, Research and Innovation Fund (NSRF via PMU-B B05F650021), Thailand; Turkish Energy, Nuclear and Mineral Research Agency (TENMAK), Turkey; National Academy of Sciences of Ukraine, Ukraine; Science and Technology Facilities Council (STFC), United Kingdom; National Science Foundation of the United States of America (NSF) and United States Department of Energy, Office of Nuclear Physics (DOE NP), United States of America. In addition, individual groups or members have received support from: European Research Council, Strong 2020 - Horizon 2020 (grant nos. 950692, 824093), European Union; Academy of Finland (Center of Excellence in Quark Matter) (grant nos. 346327, 346328), Finland.

References

- [1] E. V. Shuryak, “Event per event analysis of heavy ion collisions and thermodynamical fluctuations”, *Phys. Lett. B* **423** (1998) 9–14, arXiv:hep-ph/9704456.
- [2] M. A. Stephanov, K. Rajagopal, and E. V. Shuryak, “Event-by-event fluctuations in heavy ion collisions and the QCD critical point”, *Phys. Rev. D* **60** (1999) 114028, arXiv:hep-ph/9903292.
- [3] H. Heiselberg, “Event-by-event physics in relativistic heavy ion collisions”, *Phys. Rept.* **351** (2001) 161–194, arXiv:nucl-th/0003046.
- [4] ALICE Collaboration, “The ALICE experiment – A journey through QCD”, *CERN-EP-2022-227* (11, 2022) , arXiv:2211.04384 [nucl-ex].
- [5] E. V. Shuryak, “Quark-Gluon Plasma and Hadronic Production of Leptons, Photons and Psions”, *Phys. Lett. B* **78** (1978) 150.
- [6] L. Stodolsky, “Temperature fluctuations in multiparticle production”, *Phys. Rev. Lett.* **75** (1995) 1044–1045.

- [7] **STAR** Collaboration, J. Adams *et al.*, “Incident energy dependence of p_T correlations at RHIC”, *Phys. Rev. C* **72** (2005) 044902, arXiv:nucl-ex/0504031.
- [8] **ALICE** Collaboration, B. Abelev *et al.*, “Event-by-event mean p_T fluctuations in pp and Pb-Pb collisions at the LHC”, *Eur. Phys. J. C* **74** (2014) 3077, arXiv:1407.5530 [nucl-ex].
- [9] Z.-W. Lin, C. M. Ko, B.-A. Li, B. Zhang, and S. Pal, “A Multi-phase transport model for relativistic heavy ion collisions”, *Phys. Rev. C* **72** (2005) 064901, arXiv:nucl-th/0411110.
- [10] C. Zhang, L. Zheng, F. Liu, S. Shi, and Z.-W. Lin, “Update of a multiphase transport model with modern parton distribution functions and nuclear shadowing”, *Phys. Rev. C* **99** (2019) 064906, arXiv:1903.03292 [nucl-th].
- [11] F. Gelis, E. Iancu, J. Jalilian-Marian, and R. Venugopalan, “The Color Glass Condensate”, *Ann. Rev. Nucl. Part. Sci.* **60** (2010) 463–489, arXiv:1002.0333 [hep-ph].
- [12] H. Weigert, “Evolution at small $x(\text{bj})$: The Color glass condensate”, *Prog. Part. Nucl. Phys.* **55** (2005) 461–565, arXiv:hep-ph/0501087.
- [13] S. Gavin and G. Moschelli, “Fluctuation Probes of Early-Time Correlations in Nuclear Collisions”, *Phys. Rev. C* **85** (2012) 014905, arXiv:1107.3317 [nucl-th].
- [14] S. Bhadury, M. Kurian, V. Chandra, and A. Jaiswal, “Second order relativistic viscous hydrodynamics within an effective description of hot QCD medium”, *J. Phys. G* **48** (2021) 105104, arXiv:2010.01537 [hep-ph].
- [15] U. Heinz, C. Shen, and H. Song, “The viscosity of quark-gluon plasma at RHIC and the LHC”, *AIP Conf. Proc.* **1441** (2012) 766–770, arXiv:1108.5323 [nucl-th].
- [16] P. Romatschke, “New Developments in Relativistic Viscous Hydrodynamics”, *Int. J. Mod. Phys. E* **19** (2010) 1–53, arXiv:0902.3663 [hep-ph].
- [17] G. Giacalone, F. G. Gardim, J. Noronha-Hostler, and J.-Y. Ollitrault, “Skewness of mean transverse momentum fluctuations in heavy-ion collisions”, *Phys. Rev. C* **103** (2021) 024910, arXiv:2004.09799 [nucl-th].
- [18] F. G. Gardim, G. Giacalone, M. Luzum, and J.-Y. Ollitrault, “Effects of initial state fluctuations on the mean transverse momentum”, *Nucl. Phys. A* **1005** (2021) 121999, arXiv:2002.07008 [nucl-th].
- [19] F. G. Gardim, G. Giacalone, M. Luzum, and J.-Y. Ollitrault, “Thermodynamics of hot strong-interaction matter from ultrarelativistic nuclear collisions”, *Nature Phys.* **16** (2020) 615–619, arXiv:1908.09728 [nucl-th].
- [20] J. S. Moreland, J. E. Bernhard, and S. A. Bass, “Alternative ansatz to wounded nucleon and binary collision scaling in high-energy nuclear collisions”, *Phys. Rev. C* **92** (2015) 011901, arXiv:1412.4708 [nucl-th].
- [21] J. Noronha-Hostler, G. S. Denicol, J. Noronha, R. P. G. Andrade, and F. Grassi, “Bulk Viscosity Effects in Event-by-Event Relativistic Hydrodynamics”, *Phys. Rev. C* **88** (2013) 044916, arXiv:1305.1981 [nucl-th].
- [22] **STAR** Collaboration, S. A. Voloshin, “Multiplicity and mean transverse momentum fluctuations in Au+Au collisions at RHIC”, *AIP Conf. Proc.* **610** (2002) 591–596, arXiv:nucl-ex/0109006.

- [23] S. A. Voloshin, “Mean $p(t)$ fluctuations from two particle and four particle correlations”, arXiv:nucl-th/0206052.
- [24] ALICE Collaboration, K. Aamodt *et al.*, “The ALICE experiment at the CERN LHC”, *JINST* **3** (2008) S08002.
- [25] ALICE Collaboration, B. Abelev *et al.*, “Performance of the ALICE Experiment at the CERN LHC”, *Int. J. Mod. Phys. A* **29** (2014) 1430044, arXiv:1402.4476 [nucl-ex].
- [26] J. Alme *et al.*, “The ALICE TPC, a large 3-dimensional tracking device with fast readout for ultra-high multiplicity events”, *Nucl. Instrum. Meth. A* **622** (2010) 316–367, arXiv:1001.1950 [physics.ins-det].
- [27] ALICE Collaboration, E. Abbas *et al.*, “Performance of the ALICE VZERO system”, *JINST* **8** (2013) P10016, arXiv:1306.3130 [nucl-ex].
- [28] ALICE Collaboration, ALICE, “Centrality determination in heavy ion collisions”, *ALICE-PUBLIC-2018-011* (2018) . <http://cds.cern.ch/record/2636623>.
- [29] ALICE Collaboration, ALICE, “Centrality determination using the Glauber model in Xe-Xe collisions at $\sqrt{s_{NN}} = 5.44$ TeV”, *ALICE-PUBLIC-2018-003* (2018) . <https://cds.cern.ch/record/2315401>.
- [30] ALICE Collaboration, S. Acharya *et al.*, “Pseudorapidity distributions of charged particles as a function of mid- and forward rapidity multiplicities in pp collisions at $\sqrt{s} = 5.02, 7$ and 13 TeV”, *Eur. Phys. J. C* **81** (2021) 630, arXiv:2009.09434 [nucl-ex].
- [31] X. Luo, J. Xu, B. Mohanty, and N. Xu, “Volume fluctuation and auto-correlation effects in the moment analysis of net-proton multiplicity distributions in heavy-ion collisions”, *J. Phys. G* **40** (2013) 105104, arXiv:1302.2332 [nucl-ex].
- [32] R. Brun, F. Bruyant, F. Carminati, S. Giani, M. Maire, A. McPherson, G. Patrick, and L. Urban, “GEANT Detector Description and Simulation Tool”, *CERN-W5013* (10, 1994) . <http://cds.cern.ch/record/1082634>.
- [33] X.-N. Wang and M. Gyulassy, “HIJING: A Monte Carlo model for multiple jet production in p p, p A and A A collisions”, *Phys. Rev. D* **44** (1991) 3501–3516.
- [34] T. Sjöstrand, S. Mrenna, and P. Z. Skands, “PYTHIA 6.4 Physics and Manual”, *JHEP* **05** (2006) 026, arXiv:hep-ph/0603175.
- [35] T. Sjöstrand, S. Ask, J. R. Christiansen, R. Corke, N. Desai, P. Ilten, S. Mrenna, S. Prestel, C. O. Rasmussen, and P. Z. Skands, “An introduction to PYTHIA 8.2”, *Comput. Phys. Commun.* **191** (2015) 159–177, arXiv:1410.3012 [hep-ph].
- [36] ALICE Collaboration, J. Adam *et al.*, “Centrality dependence of the charged-particle multiplicity density at midrapidity in Pb-Pb collisions at $\sqrt{s_{NN}} = 5.02$ TeV”, *Phys. Rev. Lett.* **116** (2016) 222302, arXiv:1512.06104 [nucl-ex].
- [37] ALICE Collaboration, S. Acharya *et al.*, “Centrality and pseudorapidity dependence of the charged-particle multiplicity density in Xe–Xe collisions at $\sqrt{s_{NN}} = 5.44$ TeV”, *Phys. Lett. B* **790** (2019) 35–48, arXiv:1805.04432 [nucl-ex].
- [38] ALICE Collaboration, K. Aamodt *et al.*, “Two-pion Bose-Einstein correlations in central Pb-Pb collisions at $\sqrt{s_{NN}} = 2.76$ TeV”, *Phys. Lett. B* **696** (2011) 328–337, arXiv:1012.4035 [nucl-ex].

- [39] V. Topor Pop, M. Gyulassy, J. Barrette, C. Gale, X. N. Wang, and N. Xu, “Baryon junction loops and the baryon-meson anomaly at high energies”, *Phys. Rev. C* **70** (2004) 064906, arXiv:nucl-th/0407095.
- [40] B. Alver, M. Baker, C. Loizides, and P. Steinberg, “The PHOBOS Glauber Monte Carlo”, arXiv:0805.4411 [nucl-ex].
- [41] B. Schenke, S. Jeon, and C. Gale, “(3+1)D hydrodynamic simulation of relativistic heavy-ion collisions”, *Phys. Rev. C* **82** (2010) 014903, arXiv:1004.1408 [hep-ph].
- [42] **ALICE** Collaboration, J. Adam *et al.*, “Charged-particle multiplicities in proton–proton collisions at $\sqrt{s} = 0.9$ to 8 TeV”, *Eur. Phys. J. C* **77** (2017) 33, arXiv:1509.07541 [nucl-ex].
- [43] **ALICE** Collaboration, S. Acharya *et al.*, “Charged-particle multiplicity distributions over a wide pseudorapidity range in proton-proton collisions at $\sqrt{s} = 0.9, 7$, and 8 TeV”, *Eur. Phys. J. C* **77** (2017) 852, arXiv:1708.01435 [hep-ex].
- [44] **ALICE** Collaboration, B. Abelev *et al.*, “Multiplicity dependence of the average transverse momentum in pp, p-Pb, and Pb-Pb collisions at the LHC”, *Phys. Lett. B* **727** (2013) 371–380, arXiv:1307.1094 [nucl-ex].
- [45] T. Sjostrand and M. van Zijl, “A Multiple Interaction Model for the Event Structure in Hadron Collisions”, *Phys. Rev. D* **36** (1987) 2019.
- [46] **ALICE** Collaboration, S. Acharya *et al.*, “Transverse momentum spectra and nuclear modification factors of charged particles in pp, p-Pb and Pb-Pb collisions at the LHC”, *JHEP* **11** (2018) 013, arXiv:1802.09145 [nucl-ex].
- [47] **ALICE** Collaboration, S. Acharya *et al.*, “Transverse momentum spectra and nuclear modification factors of charged particles in Xe-Xe collisions at $\sqrt{s_{NN}} = 5.44$ TeV”, *Phys. Lett. B* **788** (2019) 166–179, arXiv:1805.04399 [nucl-ex].
- [48] R. Samanta, S. Bhatta, J. Jia, M. Luzum, and J.-Y. Ollitrault, “Thermalization at the femtoscale seen in high-energy Pb+Pb collisions”, arXiv:2303.15323 [nucl-th].
- [49] R. Samanta, J. a. P. Picchetti, M. Luzum, and J.-Y. Ollitrault, “Non-Gaussian transverse momentum fluctuations from impact parameter fluctuations”, *Phys. Rev. C* **108** (2023) 024908, arXiv:2306.09294 [nucl-th].
- [50] **ALICE** Collaboration, S. Acharya *et al.*, “Charged-particle production as a function of multiplicity and transverse spherocity in pp collisions at $\sqrt{s} = 5.02$ and 13 TeV”, *Eur. Phys. J. C* **79** (2019) 857, arXiv:1905.07208 [nucl-ex].

A The ALICE Collaboration

- S. Acharya ¹²⁸, D. Adamová ⁸⁷, G. Aglieri Rinella ³³, M. Agnello ³⁰, N. Agrawal ⁵², Z. Ahammed ¹³⁶, S. Ahmad ¹⁶, S.U. Ahn ⁷², I. Ahuja ³⁸, A. Akindinov ¹⁴², M. Al-Turany ⁹⁸, D. Aleksandrov ¹⁴², B. Alessandro ⁵⁷, H.M. Alfanda ⁶, R. Alfaro Molina ⁶⁸, B. Ali ¹⁶, A. Alici ²⁶, N. Alizadehvandchali ¹¹⁷, A. Alkin ³³, J. Alme ²¹, G. Alocco ⁵³, T. Alt ⁶⁵, A.R. Altamura ⁵¹, I. Altsybeev ⁹⁶, J.R. Alvarado ⁴⁵, M.N. Anaam ⁶, C. Andrei ⁴⁶, N. Andreou ¹¹⁶, A. Andronic ¹²⁷, V. Anguelov ⁹⁵, F. Antinori ⁵², P. Antonioli ⁵², N. Apadula ⁷⁵, L. Aphecetche ¹⁰⁴, H. Appelshäuser ⁶⁵, C. Arata ⁷⁴, S. Arcelli ²⁶, M. Aresti ²³, R. Arnaldi ⁵⁷, J.G.M.C.A. Arneiro ¹¹¹, I.C. Arsene ²⁰, M. Arslanbekov ¹³⁹, A. Augustinus ³³, R. Averbeck ⁹⁸, M.D. Azmi ¹⁶, H. Baba ¹²⁵, A. Badalà ⁵⁴, J. Bae ¹⁰⁵, Y.W. Baek ⁴¹, X. Bai ¹²¹, R. Bailhache ⁶⁵, Y. Bailung ⁴⁹, A. Balbino ³⁰, A. Baldissari ¹³¹, B. Balis ², D. Banerjee ⁴, Z. Banoo ⁹², R. Barbera ²⁷, F. Barile ³², L. Barioglio ⁹⁶, M. Barlou ⁷⁹, B. Barman ⁴², G.G. Barnaföldi ⁴⁷, L.S. Barnby ⁸⁶, V. Barret ¹²⁸, L. Barreto ¹¹¹, C. Bartels ¹²⁰, K. Barth ³³, E. Bartsch ⁶⁵, N. Bastid ¹²⁸, S. Basu ⁷⁶, G. Batigne ¹⁰⁴, D. Battistini ⁹⁶, B. Batyunya ¹⁴³, D. Bauri ⁴⁸, J.L. Bazo Alba ¹⁰², I.G. Bearden ⁸⁴, C. Beattie ¹³⁹, P. Becht ⁹⁸, D. Behera ⁴⁹, I. Belikov ¹³⁰, A.D.C. Bell Hechavarria ¹²⁷, F. Bellini ²⁶, R. Bellwied ¹¹⁷, S. Belokurova ¹⁴², Y.A.V. Beltran ⁴⁵, G. Bencedi ⁴⁷, S. Beole ²⁵, Y. Berdnikov ¹⁴², A. Berdnikova ⁹⁵, L. Bergmann ⁹⁵, M.G. Besoiu ⁶⁴, L. Betev ³³, P.P. Bhaduri ¹³⁶, A. Bhasin ⁹², M.A. Bhat ⁴, B. Bhattacharjee ⁴², L. Bianchi ²⁵, N. Bianchi ⁵⁰, J. Bielčík ³⁶, J. Bielčíková ⁸⁷, J. Biernat ¹⁰⁸, A.P. Bigot ¹³⁰, A. Bilandzic ⁹⁶, G. Biro ⁴⁷, S. Biswas ⁴, N. Bize ¹⁰⁴, J.T. Blair ¹⁰⁹, D. Blau ¹⁴², M.B. Blidaru ⁹⁸, N. Bluhme ³⁹, C. Blume ⁶⁵, G. Boca ^{22,56}, F. Bock ⁸⁸, T. Bodova ²¹, A. Bogdanov ¹⁴², S. Boi ²³, J. Bok ⁵⁹, L. Boldizsár ⁴⁷, M. Bombara ³⁸, P.M. Bond ³³, G. Bonomi ^{135,56}, H. Borel ¹³¹, A. Borissov ¹⁴², A.G. Borquez Carcamo ⁹⁵, H. Bossi ¹³⁹, E. Botta ²⁵, Y.E.M. Bouziani ⁶⁵, L. Bratrud ⁶⁵, P. Braun-Munzinger ⁹⁸, M. Bregant ¹¹¹, M. Broz ³⁶, G.E. Bruno ^{97,32}, M.D. Buckland ²⁴, D. Budnikov ¹⁴², H. Buesching ⁶⁵, S. Bufalino ³⁰, P. Buhler ¹⁰³, N. Burmasov ¹⁴², Z. Buthelezi ^{69,124}, A. Bylinkin ²¹, S.A. Bysiak ¹⁰⁸, M. Cai ⁶, H. Caines ¹³⁹, A. Caliva ²⁹, E. Calvo Villar ¹⁰², J.M.M. Camacho ¹¹⁰, P. Camerini ²⁴, F.D.M. Canedo ¹¹¹, S.L. Cantway ¹³⁹, M. Carabas ¹¹⁴, A.A. Carballo ³³, F. Carnesecchi ³³, R. Caron ¹²⁹, L.A.D. Carvalho ¹¹¹, J. Castillo Castellanos ¹³¹, F. Catalano ^{33,25}, C. Ceballos Sanchez ¹⁴³, I. Chakaberia ⁷⁵, P. Chakraborty ⁴⁸, S. Chandra ¹³⁶, S. Chapeland ³³, M. Chartier ¹²⁰, S. Chattopadhyay ¹³⁶, S. Chattopadhyay ¹⁰⁰, T. Cheng ^{98,6}, C. Cheshkov ¹²⁹, B. Cheynis ¹²⁹, V. Chibante Barroso ³³, D.D. Chinellato ¹¹², E.S. Chizzali ^{II,96}, J. Cho ⁵⁹, S. Cho ⁵⁹, P. Chochula ³³, D. Choudhury ⁴², P. Christakoglou ⁸⁵, C.H. Christensen ⁸⁴, P. Christiansen ⁷⁶, T. Chujo ¹²⁶, M. Ciacco ³⁰, C. Cicalo ⁵³, F. Cindolo ⁵², M.R. Ciupek ⁹⁸, G. Clai III,52, F. Colamaria ⁵¹, J.S. Colburn ¹⁰¹, D. Colella ^{97,32}, M. Colocci ²⁶, M. Concias ^{IV,33}, G. Conesa Balbastre ⁷⁴, Z. Conesa del Valle ¹³², G. Contin ²⁴, J.G. Contreras ³⁶, M.L. Coquet ¹³¹, P. Cortese ^{134,57}, M.R. Cosentino ¹¹³, F. Costa ³³, S. Costanza ^{22,56}, C. Cot ¹³², J. Crkovská ⁹⁵, P. Crochet ¹²⁸, R. Cruz-Torres ⁷⁵, P. Cui ⁶, A. Dainese ⁵⁵, M.C. Danisch ⁹⁵, A. Danu ⁶⁴, P. Das ⁸¹, P. Das ⁴, S. Das ⁴, A.R. Dash ¹²⁷, S. Dash ⁴⁸, A. De Caro ²⁹, G. de Cataldo ⁵¹, J. de Cuveland ³⁹, A. De Falco ²³, D. De Gruttola ²⁹, N. De Marco ⁵⁷, C. De Martin ²⁴, S. De Pasquale ²⁹, R. Deb ¹³⁵, R. Del Grande ⁹⁶, L. Dello Stritto ²⁹, W. Deng ⁶, P. Dhankher ¹⁹, D. Di Bari ³², A. Di Mauro ³³, B. Diab ¹³¹, R.A. Diaz ^{143,7}, T. Dietel ¹¹⁵, Y. Ding ⁶, J. Ditzel ⁶⁵, R. Divià ³³, D.U. Dixit ¹⁹, Ø. Djupsland ²¹, U. Dmitrieva ¹⁴², A. Dobrin ⁶⁴, B. Dönigus ⁶⁵, J.M. Dubinski ¹³⁷, A. Dubla ⁹⁸, S. Dudi ⁹¹, P. Dupieux ¹²⁸, M. Durkac ¹⁰⁷, N. Dzalaiova ¹³, T.M. Eder ¹²⁷, R.J. Ehlers ⁷⁵, F. Eisenhut ⁶⁵, R. Ejima ⁹³, D. Elia ⁵¹, B. Erazmus ¹⁰⁴, F. Ercolelli ²⁶, B. Espagnon ¹³², G. Eulisse ³³, D. Evans ¹⁰¹, S. Evdokimov ¹⁴², L. Fabbietti ⁹⁶, M. Faggion ²⁸, J. Faivre ⁷⁴, F. Fan ⁶, W. Fan ⁷⁵, A. Fantoni ⁵⁰, M. Fasel ⁸⁸, A. Feliciello ⁵⁷, G. Feofilov ¹⁴², A. Fernández Téllez ⁴⁵, L. Ferrandi ¹¹¹, M.B. Ferrer ³³, A. Ferrero ¹³¹, C. Ferrero ⁵⁷, A. Ferretti ²⁵, V.J.G. Feuillard ⁹⁵, V. Filova ³⁶, D. Finogeev ¹⁴², F.M. Fionda ⁵³, E. Flatland ³³, F. Flor ¹¹⁷, A.N. Flores ¹⁰⁹, S. Foertsch ⁶⁹, I. Fokin ⁹⁵, S. Fokin ¹⁴², E. Fragiocomo ⁵⁸, E. Frajna ⁴⁷, U. Fuchs ³³, N. Funicello ²⁹, C. Furget ⁷⁴, A. Furs ¹⁴², T. Fusayasu ⁹⁹, J.J. Gaardhøje ⁸⁴, M. Gagliardi ²⁵, A.M. Gago ¹⁰², T. Gahlaud ⁴⁸, C.D. Galvan ¹¹⁰, D.R. Gangadharan ¹¹⁷, P. Ganoti ⁷⁹, C. Garabatos ⁹⁸, T. García Chávez ⁴⁵, E. Garcia-Solis ⁹, C. Gargiulo ³³, P. Gasik ⁹⁸, A. Gautam ¹¹⁹, M.B. Gay Ducati ⁶⁷, M. Germain ¹⁰⁴, A. Ghimouz ¹²⁶, C. Ghosh ¹³⁶, M. Giacalone ⁵², G. Gioachin ³⁰, P. Giubellino ^{98,57}, P. Giubilato ²⁸, A.M.C. Glaenzer ¹³¹, P. Glässel ⁹⁵, E. Glimos ¹²³, D.J.Q. Goh ⁷⁷, V. Gonzalez ¹³⁸, P. Gordeev ¹⁴², M. Gorgon ², K. Goswami ⁴⁹, S. Gotovac ³⁴, V. Grabski ⁶⁸, L.K. Graczykowski ¹³⁷, E. Grecka ⁸⁷, A. Grelli ⁶⁰, C. Grigoras ³³, V. Grigoriev ¹⁴², S. Grigoryan ^{143,1}, F. Grossa ³³, J.F. Grosse-Oetringhaus ³³, R. Grossi ⁹⁸, D. Grund ³⁶, N.A. Grunwald ⁹⁵, G.G. Guardiano ¹¹², R. Guernane ⁷⁴, M. Guilbaud ¹⁰⁴,

- K. Gulbrandsen⁸⁴, T. Gündem⁶⁵, T. Gunji¹²⁵, W. Guo⁶, A. Gupta⁹², R. Gupta⁹², R. Gupta⁴⁹, K. Gwizdziel¹³⁷, L. Gyulai⁴⁷, C. Hadjidakis¹³², F.U. Haider⁹², S. Haidlova³⁶, H. Hamagaki⁷⁷, A. Hamdi⁷⁵, Y. Han¹⁴⁰, B.G. Hanley¹³⁸, R. Hannigan¹⁰⁹, J. Hansen⁷⁶, M.R. Haque¹³⁷, J.W. Harris¹³⁹, A. Harton⁹, H. Hassan¹¹⁸, D. Hatzifotiadou⁵², P. Hauer⁴³, L.B. Havener¹³⁹, S.T. Heckel⁹⁶, E. Hellbär⁹⁸, H. Helstrup³⁵, M. Hemmer⁶⁵, T. Herman³⁶, G. Herrera Corral⁸, F. Herrmann¹²⁷, S. Herrmann¹²⁹, K.F. Hetland³⁵, B. Heybeck⁶⁵, H. Hillemanns³³, B. Hippolyte¹³⁰, F.W. Hoffmann⁷¹, B. Hofman⁶⁰, G.H. Hong¹⁴⁰, M. Horst⁹⁶, A. Horzyk², Y. Hou⁶, P. Hristov³³, C. Hughes¹²³, P. Huhn⁶⁵, L.M. Huhta¹¹⁸, T.J. Humanic⁸⁹, A. Hutson¹¹⁷, D. Hutter³⁹, R. Ilkaev¹⁴², H. Ilyas¹⁴, M. Inaba¹²⁶, G.M. Innocenti³³, M. Ippolitov¹⁴², A. Isakov^{85,87}, T. Isidori¹¹⁹, M.S. Islam¹⁰⁰, M. Ivanov¹³, M. Ivanov⁹⁸, V. Ivanov¹⁴², K.E. Iversen⁷⁶, M. Jablonski², B. Jacak⁷⁵, N. Jacazio²⁶, P.M. Jacobs⁷⁵, S. Jadlovska¹⁰⁷, J. Jadlovsky¹⁰⁷, S. Jaelani⁸³, C. Jahnke¹¹¹, M.J. Jakubowska¹³⁷, M.A. Janik¹³⁷, T. Janson⁷¹, S. Ji¹⁷, S. Jia¹⁰, A.A.P. Jimenez⁶⁶, F. Jonas^{88,127}, D.M. Jones¹²⁰, J.M. Jowett^{33,98}, J. Jung⁶⁵, M. Jung⁶⁵, A. Junique³³, A. Jusko¹⁰¹, M.J. Kabus^{33,137}, J. Kaewjai¹⁰⁶, P. Kalinak⁶¹, A.S. Kalteyer⁹⁸, A. Kalweit³³, V. Kaplin¹⁴², A. Karasu Uysal⁷³, D. Karatovic⁹⁰, O. Karavichev¹⁴², T. Karavicheva¹⁴², P. Karczmarczyk¹³⁷, E. Karpechev¹⁴², U. Kebschull⁷¹, R. Keidel¹⁴¹, D.L.D. Keijdener⁶⁰, M. Keil³³, B. Ketzer⁴³, S.S. Khade⁴⁹, A.M. Khan¹²¹, S. Khan¹⁶, A. Khanzadeev¹⁴², Y. Kharlov¹⁴², A. Khatun¹¹⁹, A. Khuntia³⁶, B. Kileng³⁵, B. Kim¹⁰⁵, C. Kim¹⁷, D.J. Kim¹¹⁸, E.J. Kim⁷⁰, J. Kim¹⁴⁰, J.S. Kim⁴¹, J. Kim⁵⁹, J. Kim⁷⁰, M. Kim¹⁹, S. Kim¹⁸, T. Kim¹⁴⁰, K. Kimura⁹³, S. Kirsch⁶⁵, I. Kisel³⁹, S. Kiselev¹⁴², A. Kisiel¹³⁷, J.P. Kitowski², J.L. Klay⁵, J. Klein³³, S. Klein⁷⁵, C. Klein-Bösing¹²⁷, M. Kleiner⁶⁵, T. Klemenz⁹⁶, A. Kluge³³, A.G. Knospe¹¹⁷, C. Kobdaj¹⁰⁶, T. Kollegger⁹⁸, A. Kondratyev¹⁴³, N. Kondratyeva¹⁴², E. Kondratyuk¹⁴², J. Konig⁶⁵, S.A. Konigstorfer⁹⁶, P.J. Konopka³³, G. Kornakov¹³⁷, M. Korwieser⁹⁶, S.D. Koryciak², A. Kotliarov⁸⁷, V. Kovalenko¹⁴², M. Kowalski¹⁰⁸, V. Kozhuharov³⁷, I. Králik⁶¹, A. Kravčáková³⁸, L. Krcal^{33,39}, M. Krivda^{101,61}, F. Krizek⁸⁷, K. Krizkova Gajdosova³³, M. Kroesen⁹⁵, M. Krüger⁶⁵, D.M. Krupova³⁶, E. Kryshen¹⁴², V. Kućera⁵⁹, C. Kuhn¹³⁰, P.G. Kuijer⁸⁵, T. Kumaoka¹²⁶, D. Kumar¹³⁶, L. Kumar⁹¹, N. Kumar⁹¹, S. Kumar³², S. Kundu³³, P. Kurashvili⁸⁰, A. Kurepin¹⁴², A.B. Kurepin¹⁴², A. Kuryakin¹⁴², S. Kushpil⁸⁷, V. Kuskov¹⁴², M.J. Kweon⁵⁹, Y. Kwon¹⁴⁰, S.L. La Pointe³⁹, P. La Rocca²⁷, A. Lakrathok¹⁰⁶, M. Lamanna³³, A.R. Landou^{74,116}, R. Langoy¹²², P. Larionov³³, E. Laudi³³, L. Lautner^{33,96}, R. Lavicka¹⁰³, R. Lea^{135,56}, H. Lee¹⁰⁵, I. Legrand⁴⁶, G. Legras¹²⁷, J. Lehrbach³⁹, T.M. Lelek², R.C. Lemmon⁸⁶, I. León Monzón¹¹⁰, M.M. Lesch⁹⁶, E.D. Lesser¹⁹, P. Lévai⁴⁷, X. Li¹⁰, J. Lien¹²², R. Lietava¹⁰¹, I. Likmeta¹¹⁷, B. Lim²⁵, S.H. Lim¹⁷, V. Lindenstruth³⁹, A. Lindner⁴⁶, C. Lippmann⁹⁸, D.H. Liu⁶, J. Liu¹²⁰, G.S.S. Liveraro¹¹², I.M. Lofnes²¹, C. Loizides⁸⁸, S. Lokos¹⁰⁸, J. Lömkér⁶⁰, P. Loncar³⁴, X. Lopez¹²⁸, E. López Torres⁷, P. Lu^{98,121}, F.V. Lugo⁶⁸, J.R. Luhder¹²⁷, M. Lunardon²⁸, G. Luparello⁵⁸, Y.G. Ma⁴⁰, M. Mager³³, A. Maire¹³⁰, E.M. Majerz², M.V. Makariev³⁷, M. Malaev¹⁴², G. Malfattore²⁶, N.M. Malik⁹², Q.W. Malik²⁰, S.K. Malik⁹², L. Malinina^{I,VII,143}, D. Mallick^{132,81}, N. Mallick⁴⁹, G. Mandaglio^{31,54}, S.K. Mandal⁸⁰, V. Manko¹⁴², F. Manso¹²⁸, V. Manzari⁵¹, Y. Mao⁶, R.W. Marcjan², G.V. Margagliotti²⁴, A. Margotti⁵², A. Marín⁹⁸, C. Markert¹⁰⁹, P. Martinengo³³, M.I. Martínez⁴⁵, G. Martínez García¹⁰⁴, M.P.P. Martins¹¹¹, S. Masciocchi⁹⁸, M. Masera²⁵, A. Masoni⁵³, L. Massacrier¹³², O. Massen⁶⁰, A. Mastroserio^{133,51}, O. Matonoha⁷⁶, S. Mattiazzo²⁸, A. Matyja¹⁰⁸, C. Mayer¹⁰⁸, A.L. Mazuecos³³, F. Mazzaschi²⁵, M. Mazzilli³³, J.E. Mdhluli¹²⁴, Y. Melikyan⁴⁴, A. Menchaca-Rocha⁶⁸, J.E.M. Mendez⁶⁶, E. Meninno¹⁰³, A.S. Menon¹¹⁷, M. Meres¹³, S. Mhlanga^{115,69}, Y. Miake¹²⁶, L. Micheletti³³, D.L. Mihaylov⁹⁶, K. Mikhaylov^{143,142}, A.N. Mishra⁴⁷, D. Miśkowiec⁹⁸, A. Modak⁴, B. Mohanty⁸¹, M. Mohisin Khan^{V,16}, M.A. Molander⁴⁴, S. Monira¹³⁷, C. Mordasini¹¹⁸, D.A. Moreira De Godoy¹²⁷, I. Morozov¹⁴², A. Morsch³³, T. Mrnjavac³³, V. Muccifora⁵⁰, S. Muhuri¹³⁶, J.D. Mulligan⁷⁵, A. Mulliri²³, M.G. Munhoz¹¹¹, R.H. Munzer⁶⁵, H. Murakami¹²⁵, S. Murray¹¹⁵, L. Musa³³, J. Musinsky⁶¹, J.W. Myrcha¹³⁷, B. Naik¹²⁴, A.I. Nambrath¹⁹, B.K. Nandi⁴⁸, R. Nania⁵², E. Nappi⁵¹, A.F. Nassirpour¹⁸, A. Nath⁹⁵, C. Natrass¹²³, T.K. Nayak^{81,117}, M.N. Naydenov³⁷, A. Neagu²⁰, A. Negru¹¹⁴, E. Nekrasova¹⁴², L. Nellen⁶⁶, R. Nepeivoda⁷⁶, S. Nese²⁰, G. Neskovic³⁹, N. Nicassio⁵¹, B.S. Nielsen⁸⁴, E.G. Nielsen⁸⁴, S. Nikolaev¹⁴², S. Nikulin¹⁴², V. Nikulin¹⁴², F. Noferini⁵², S. Noh¹², P. Nomokonov¹⁴³, J. Norman¹²⁰, N. Novitzky⁸⁸, P. Nowakowski¹³⁷, A. Nyanin¹⁴², J. Nystrand²¹, M. Ogino⁷⁷, S. Oh¹⁸, A. Ohlson⁷⁶, V.A. Okorokov¹⁴², J. Oleniacz¹³⁷, A.C. Oliveira Da Silva¹²³, A. Onnerstad¹¹⁸, C. Oppedisano⁵⁷, A. Ortiz Velasquez⁶⁶, J. Otwinowski¹⁰⁸, M. Oya⁹³, K. Oyama⁷⁷, Y. Pachmayer⁹⁵, S. Padhan⁴⁸, D. Pagano^{135,56}, G. Paić⁶⁶, S. Paisano-Guzmán⁴⁵,

- A. Palasciano ⁵¹, S. Panebianco ¹³¹, H. Park ¹²⁶, H. Park ¹⁰⁵, J. Park ⁵⁹, J.E. Parkkila ³³, Y. Patley ⁴⁸, R.N. Patra ⁹², B. Paul ²³, H. Pei ⁶, T. Peitzmann ⁶⁰, X. Peng ¹¹, M. Pennisi ²⁵, S. Perciballi ²⁵, D. Peresunko ¹⁴², G.M. Perez ⁷, Y. Pestov ¹⁴², V. Petrov ¹⁴², M. Petrovici ⁴⁶, R.P. Pezzi ^{104,67}, S. Piano ⁵⁸, M. Pikna ¹³, P. Pillot ¹⁰⁴, O. Pinazza ^{52,33}, L. Pinsky ¹¹⁷, C. Pinto ⁹⁶, S. Pisano ⁵⁰, M. Płoskoń ⁷⁵, M. Planinic ⁹⁰, F. Pliquet ⁶⁵, M.G. Poghosyan ⁸⁸, B. Polichtchouk ¹⁴², S. Politano ³⁰, N. Poljak ⁹⁰, A. Pop ⁴⁶, S. Porteboeuf-Houssais ¹²⁸, V. Pozdniakov ¹⁴³, I.Y. Pozos ⁴⁵, K.K. Pradhan ⁴⁹, S.K. Prasad ⁴, S. Prasad ⁴⁹, R. Preghenella ⁵², F. Prino ⁵⁷, C.A. Pruneau ¹³⁸, I. Pshenichnov ¹⁴², M. Puccio ³³, S. Pucillo ²⁵, Z. Pugelova ¹⁰⁷, S. Qiu ⁸⁵, L. Quaglia ²⁵, S. Ragoni ¹⁵, A. Rai ¹³⁹, A. Rakotozafindrabe ¹³¹, L. Ramello ^{134,57}, F. Rami ¹³⁰, T.A. Rancien ⁷⁴, M. Rasa ²⁷, S.S. Räsänen ⁴⁴, R. Rath ⁵², M.P. Rauch ²¹, I. Ravasenga ⁸⁵, K.F. Read ^{88,123}, C. Reckziegel ¹¹³, A.R. Redelbach ³⁹, K. Redlich ^{VI,80}, C.A. Reetz ⁹⁸, H.D. Regules-Medel ⁴⁵, A. Rehman ²¹, F. Reidt ³³, H.A. Reme-Ness ³⁵, Z. Rescakova ³⁸, K. Reygers ⁹⁵, A. Riabov ¹⁴², V. Riabov ¹⁴², R. Ricci ²⁹, M. Richter ²⁰, A.A. Riedel ⁹⁶, W. Riegler ³³, A.G. Riffero ²⁵, C. Ristea ⁶⁴, M.V. Rodriguez ³³, M. Rodríguez Cahuantzi ⁴⁵, S.A. Rodríguez Ramírez ⁴⁵, K. Røed ²⁰, R. Rogalev ¹⁴², E. Rogochaya ¹⁴³, T.S. Rogoschinski ⁶⁵, D. Rohr ³³, D. Röhrich ²¹, P.F. Rojas ⁴⁵, S. Rojas Torres ³⁶, P.S. Rokita ¹³⁷, G. Romanenko ²⁶, F. Ronchetti ⁵⁰, A. Rosano ^{31,54}, E.D. Rosas ⁶⁶, K. Roslon ¹³⁷, A. Rossi ⁵⁵, A. Roy ⁴⁹, S. Roy ⁴⁸, N. Rubini ²⁶, D. Ruggiano ¹³⁷, R. Rui ²⁴, P.G. Russek ², R. Russo ⁸⁵, A. Rustamov ⁸², E. Ryabinkin ¹⁴², Y. Ryabov ¹⁴², A. Rybicki ¹⁰⁸, H. Rytkonen ¹¹⁸, J. Ryu ¹⁷, W. Rzesz ¹³⁷, O.A.M. Saarimaki ⁴⁴, S. Sadhu ³², S. Sadovsky ¹⁴², J. Saetre ²¹, K. Šafářík ³⁶, P. Saha ⁴², S.K. Saha ⁴, S. Saha ⁸¹, B. Sahoo ⁴⁸, B. Sahoo ⁴⁹, R. Sahoo ⁴⁹, S. Sahoo ⁶², D. Sahu ⁴⁹, P.K. Sahu ⁶², J. Saini ¹³⁶, K. Sajdakova ³⁸, S. Sakai ¹²⁶, M.P. Salvan ⁹⁸, S. Sambyal ⁹², D. Samitz ¹⁰³, I. Sanna ^{33,96}, T.B. Saramela ¹¹¹, P. Sarma ⁴², V. Sarritzu ²³, V.M. Sarti ⁹⁶, M.H.P. Sas ³³, S. Sawan ⁸¹, J. Schambach ⁸⁸, H.S. Scheid ⁶⁵, C. Schiaua ⁴⁶, R. Schicker ⁹⁵, F. Schlepper ⁹⁵, A. Schmeh ⁹⁸, C. Schmidt ⁹⁸, H.R. Schmidt ⁹⁴, M.O. Schmidt ³³, M. Schmidt ⁹⁴, N.V. Schmidt ⁸⁸, A.R. Schmier ¹²³, R. Schotter ¹³⁰, A. Schröter ³⁹, J. Schukraft ³³, K. Schweda ⁹⁸, G. Scioli ²⁶, E. Scomparin ⁵⁷, J.E. Seger ¹⁵, Y. Sekiguchi ¹²⁵, D. Sekihata ¹²⁵, M. Selina ⁸⁵, I. Selyuzhenkov ⁹⁸, S. Senyukov ¹³⁰, J.J. Seo ^{95,59}, D. Serebryakov ¹⁴², L. Šerkšnytė ⁹⁶, A. Sevcenco ⁶⁴, T.J. Shaba ⁶⁹, A. Shabetai ¹⁰⁴, R. Shahoyan ³³, A. Shangaraev ¹⁴², A. Sharma ⁹¹, B. Sharma ⁹², D. Sharma ⁴⁸, H. Sharma ⁵⁵, M. Sharma ⁹², S. Sharma ⁷⁷, S. Sharma ⁹², U. Sharma ⁹², A. Shatat ¹³², O. Sheibani ¹¹⁷, K. Shigaki ⁹³, M. Shimomura ⁷⁸, J. Shin ¹², S. Shirinkin ¹⁴², Q. Shou ⁴⁰, Y. Sibiriak ¹⁴², S. Siddhanta ⁵³, T. Siemarczuk ⁸⁰, T.F. Silva ¹¹¹, D. Silvermyr ⁷⁶, T. Simantathammakul ¹⁰⁶, R. Simeonov ³⁷, B. Singh ⁹², B. Singh ⁹⁶, K. Singh ⁴⁹, R. Singh ⁸¹, R. Singh ⁹², R. Singh ⁴⁹, S. Singh ¹⁶, V.K. Singh ¹³⁶, V. Singhal ¹³⁶, T. Sinha ¹⁰⁰, B. Sitar ¹³, M. Sitta ^{134,57}, T.B. Skaali ²⁰, G. Skorodumovs ⁹⁵, M. Slupecki ⁴⁴, N. Smirnov ¹³⁹, R.J.M. Snellings ⁶⁰, E.H. Solheim ²⁰, J. Song ¹⁷, C. Sonnabend ^{33,98}, F. Soramel ²⁸, A.B. Soto-hernandez ⁸⁹, R. Spijkers ⁸⁵, I. Sputowska ¹⁰⁸, J. Staa ⁷⁶, J. Stachel ⁹⁵, I. Stan ⁶⁴, P.J. Steffanic ¹²³, S.F. Stiefelmaier ⁹⁵, D. Stocco ¹⁰⁴, I. Storehaug ²⁰, P. Stratmann ¹²⁷, S. Strazzi ²⁶, A. Sturniolo ^{31,54}, C.P. Stylianidis ⁸⁵, A.A.P. Suwaide ¹¹¹, C. Suire ¹³², M. Sukhanov ¹⁴², M. Suljic ³³, R. Sultanov ¹⁴², V. Sumberia ⁹², S. Sumowidago ⁸³, S. Swain ⁶², I. Szarka ¹³, M. Szymkowski ¹³⁷, S.F. Taghavi ⁹⁶, G. Taillepied ⁹⁸, J. Takahashi ¹¹², G.J. Tambave ⁸¹, S. Tang ⁶, Z. Tang ¹²¹, J.D. Tapia Takaki ¹¹⁹, N. Tapus ¹¹⁴, L.A. Tarasovicova ¹²⁷, M.G. Tarzila ⁴⁶, G.F. Tassielli ³², A. Tauro ³³, A. Tavira García ¹³², G. Tejeda Muñoz ⁴⁵, A. Telesca ³³, L. Terlizzi ²⁵, C. Terrevoli ¹¹⁷, S. Thakur ⁴, D. Thomas ¹⁰⁹, A. Tikhonov ¹⁴², N. Tiltmann ¹²⁷, A.R. Timmins ¹¹⁷, M. Tkacik ¹⁰⁷, T. Tkacik ¹⁰⁷, A. Toia ⁶⁵, R. Tokumoto ⁹³, K. Tomohiro ⁹³, N. Topilskaya ¹⁴², M. Toppi ⁵⁰, T. Tork ¹³², V.V. Torres ¹⁰⁴, A.G. Torres Ramos ³², A. Trifiró ^{31,54}, A.S. Triolo ^{33,31,54}, S. Tripathy ⁵², T. Tripathy ⁴⁸, S. Trogolo ³³, V. Trubnikov ³, W.H. Trzaska ¹¹⁸, T.P. Trzciński ¹³⁷, A. Tumkin ¹⁴², R. Turrisi ⁵⁵, T.S. Tveter ²⁰, K. Ullaland ²¹, B. Ulukutlu ⁹⁶, A. Uras ¹²⁹, G.L. Usai ²³, M. Vala ³⁸, N. Valle ²², L.V.R. van Doremalen ⁶⁰, M. van Leeuwen ⁸⁵, C.A. van Veen ⁹⁵, R.J.G. van Weelden ⁸⁵, P. Vande Vyvre ³³, D. Varga ⁴⁷, Z. Varga ⁴⁷, P. Vargas Torres ⁶⁶, M. Vasileiou ⁷⁹, A. Vasiliev ¹⁴², O. Vázquez Doce ⁵⁰, O. Vazquez Rueda ¹¹⁷, V. Vechernin ¹⁴², E. Vercellin ²⁵, S. Vergara Limón ⁴⁵, R. Verma ⁴⁸, L. Vermunt ⁹⁸, R. Vértesi ⁴⁷, M. Verweij ⁶⁰, L. Vickovic ³⁴, Z. Vilakazi ¹²⁴, O. Villalobos Baillie ¹⁰¹, A. Villani ²⁴, A. Vinogradov ¹⁴², T. Virgili ²⁹, M.M.O. Virta ¹¹⁸, V. Vislavicius ⁷⁶, A. Vodopyanov ¹⁴³, B. Volkel ³³, M.A. Völkl ⁹⁵, K. Voloshin ¹⁴², S.A. Voloshin ¹³⁸, G. Volpe ³², B. von Haller ³³, I. Vorobyev ⁹⁶, N. Vozniuk ¹⁴², J. Vrláková ³⁸, J. Wan ⁴⁰, C. Wang ⁴⁰, D. Wang ⁴⁰, Y. Wang ⁴⁰, Y. Wang ⁶, A. Wegrynek ³³, F.T. Weiglhofer ³⁹, S.C. Wenzel ³³, J.P. Wessels ¹²⁷, J. Wiechula ⁶⁵, J. Wikne ²⁰, G. Wilk ⁸⁰, J. Wilkinson ⁹⁸, G.A. Willems ¹²⁷, B. Windelband ⁹⁵, M. Winn ¹³¹, J.R. Wright ¹⁰⁹, W. Wu ⁴⁰, Y. Wu ¹²¹, R. Xu ⁶, A. Yadav ⁴³, A.K. Yadav ¹³⁶,

S. Yalcin ⁷³, Y. Yamaguchi ⁹³, S. Yang²¹, S. Yano ⁹³, Z. Yin ⁶, I.-K. Yoo ¹⁷, J.H. Yoon ⁵⁹, H. Yu¹²,
 S. Yuan²¹, A. Yuncu ⁹⁵, V. Zaccolo ²⁴, C. Zampolli ³³, F. Zanone ⁹⁵, N. Zardoshti ³³,
 A. Zarochentsev ¹⁴², P. Závada ⁶³, N. Zaviyalov¹⁴², M. Zhalov ¹⁴², B. Zhang ⁶, C. Zhang ¹³¹,
 L. Zhang ⁴⁰, S. Zhang ⁴⁰, X. Zhang ⁶, Y. Zhang¹²¹, Z. Zhang ⁶, M. Zhao ¹⁰, V. Zherebchevskii ¹⁴²,
 Y. Zhi¹⁰, D. Zhou ⁶, Y. Zhou ⁸⁴, J. Zhu ^{55,6}, Y. Zhu⁶, S.C. Zugravel ⁵⁷, N. Zurlo ^{135,56}

Affiliation Notes

^I Deceased

^{II} Also at: Max-Planck-Institut fur Physik, Munich, Germany

^{III} Also at: Italian National Agency for New Technologies, Energy and Sustainable Economic Development (ENEA), Bologna, Italy

^{IV} Also at: Dipartimento DET del Politecnico di Torino, Turin, Italy

^V Also at: Department of Applied Physics, Aligarh Muslim University, Aligarh, India

^{VI} Also at: Institute of Theoretical Physics, University of Wroclaw, Poland

^{VII} Also at: An institution covered by a cooperation agreement with CERN

Collaboration Institutes

¹ A.I. Alikhanyan National Science Laboratory (Yerevan Physics Institute) Foundation, Yerevan, Armenia

² AGH University of Krakow, Cracow, Poland

³ Bogolyubov Institute for Theoretical Physics, National Academy of Sciences of Ukraine, Kiev, Ukraine

⁴ Bose Institute, Department of Physics and Centre for Astroparticle Physics and Space Science (CAPSS), Kolkata, India

⁵ California Polytechnic State University, San Luis Obispo, California, United States

⁶ Central China Normal University, Wuhan, China

⁷ Centro de Aplicaciones Tecnológicas y Desarrollo Nuclear (CEADEN), Havana, Cuba

⁸ Centro de Investigación y de Estudios Avanzados (CINVESTAV), Mexico City and Mérida, Mexico

⁹ Chicago State University, Chicago, Illinois, United States

¹⁰ China Institute of Atomic Energy, Beijing, China

¹¹ China University of Geosciences, Wuhan, China

¹² Chungbuk National University, Cheongju, Republic of Korea

¹³ Comenius University Bratislava, Faculty of Mathematics, Physics and Informatics, Bratislava, Slovak Republic

¹⁴ COMSATS University Islamabad, Islamabad, Pakistan

¹⁵ Creighton University, Omaha, Nebraska, United States

¹⁶ Department of Physics, Aligarh Muslim University, Aligarh, India

¹⁷ Department of Physics, Pusan National University, Pusan, Republic of Korea

¹⁸ Department of Physics, Sejong University, Seoul, Republic of Korea

¹⁹ Department of Physics, University of California, Berkeley, California, United States

²⁰ Department of Physics, University of Oslo, Oslo, Norway

²¹ Department of Physics and Technology, University of Bergen, Bergen, Norway

²² Dipartimento di Fisica, Università di Pavia, Pavia, Italy

²³ Dipartimento di Fisica dell'Università and Sezione INFN, Cagliari, Italy

²⁴ Dipartimento di Fisica dell'Università and Sezione INFN, Trieste, Italy

²⁵ Dipartimento di Fisica dell'Università and Sezione INFN, Turin, Italy

²⁶ Dipartimento di Fisica e Astronomia dell'Università and Sezione INFN, Bologna, Italy

²⁷ Dipartimento di Fisica e Astronomia dell'Università and Sezione INFN, Catania, Italy

²⁸ Dipartimento di Fisica e Astronomia dell'Università and Sezione INFN, Padova, Italy

²⁹ Dipartimento di Fisica 'E.R. Caianiello' dell'Università and Gruppo Collegato INFN, Salerno, Italy

³⁰ Dipartimento DISAT del Politecnico and Sezione INFN, Turin, Italy

³¹ Dipartimento di Scienze MIFT, Università di Messina, Messina, Italy

³² Dipartimento Interateneo di Fisica 'M. Merlin' and Sezione INFN, Bari, Italy

³³ European Organization for Nuclear Research (CERN), Geneva, Switzerland

³⁴ Faculty of Electrical Engineering, Mechanical Engineering and Naval Architecture, University of Split, Split, Croatia

³⁵ Faculty of Engineering and Science, Western Norway University of Applied Sciences, Bergen, Norway

- ³⁶ Faculty of Nuclear Sciences and Physical Engineering, Czech Technical University in Prague, Prague, Czech Republic
- ³⁷ Faculty of Physics, Sofia University, Sofia, Bulgaria
- ³⁸ Faculty of Science, P.J. Šafárik University, Košice, Slovak Republic
- ³⁹ Frankfurt Institute for Advanced Studies, Johann Wolfgang Goethe-Universität Frankfurt, Frankfurt, Germany
- ⁴⁰ Fudan University, Shanghai, China
- ⁴¹ Gangneung-Wonju National University, Gangneung, Republic of Korea
- ⁴² Gauhati University, Department of Physics, Guwahati, India
- ⁴³ Helmholtz-Institut für Strahlen- und Kernphysik, Rheinische Friedrich-Wilhelms-Universität Bonn, Bonn, Germany
- ⁴⁴ Helsinki Institute of Physics (HIP), Helsinki, Finland
- ⁴⁵ High Energy Physics Group, Universidad Autónoma de Puebla, Puebla, Mexico
- ⁴⁶ Horia Hulubei National Institute of Physics and Nuclear Engineering, Bucharest, Romania
- ⁴⁷ HUN-REN Wigner Research Centre for Physics, Budapest, Hungary
- ⁴⁸ Indian Institute of Technology Bombay (IIT), Mumbai, India
- ⁴⁹ Indian Institute of Technology Indore, Indore, India
- ⁵⁰ INFN, Laboratori Nazionali di Frascati, Frascati, Italy
- ⁵¹ INFN, Sezione di Bari, Bari, Italy
- ⁵² INFN, Sezione di Bologna, Bologna, Italy
- ⁵³ INFN, Sezione di Cagliari, Cagliari, Italy
- ⁵⁴ INFN, Sezione di Catania, Catania, Italy
- ⁵⁵ INFN, Sezione di Padova, Padova, Italy
- ⁵⁶ INFN, Sezione di Pavia, Pavia, Italy
- ⁵⁷ INFN, Sezione di Torino, Turin, Italy
- ⁵⁸ INFN, Sezione di Trieste, Trieste, Italy
- ⁵⁹ Inha University, Incheon, Republic of Korea
- ⁶⁰ Institute for Gravitational and Subatomic Physics (GRASP), Utrecht University/Nikhef, Utrecht, Netherlands
- ⁶¹ Institute of Experimental Physics, Slovak Academy of Sciences, Košice, Slovak Republic
- ⁶² Institute of Physics, Homi Bhabha National Institute, Bhubaneswar, India
- ⁶³ Institute of Physics of the Czech Academy of Sciences, Prague, Czech Republic
- ⁶⁴ Institute of Space Science (ISS), Bucharest, Romania
- ⁶⁵ Institut für Kernphysik, Johann Wolfgang Goethe-Universität Frankfurt, Frankfurt, Germany
- ⁶⁶ Instituto de Ciencias Nucleares, Universidad Nacional Autónoma de México, Mexico City, Mexico
- ⁶⁷ Instituto de Física, Universidade Federal do Rio Grande do Sul (UFRGS), Porto Alegre, Brazil
- ⁶⁸ Instituto de Física, Universidad Nacional Autónoma de México, Mexico City, Mexico
- ⁶⁹ iThemba LABS, National Research Foundation, Somerset West, South Africa
- ⁷⁰ Jeonbuk National University, Jeonju, Republic of Korea
- ⁷¹ Johann-Wolfgang-Goethe Universität Frankfurt Institut für Informatik, Fachbereich Informatik und Mathematik, Frankfurt, Germany
- ⁷² Korea Institute of Science and Technology Information, Daejeon, Republic of Korea
- ⁷³ KTO Karatay University, Konya, Turkey
- ⁷⁴ Laboratoire de Physique Subatomique et de Cosmologie, Université Grenoble-Alpes, CNRS-IN2P3, Grenoble, France
- ⁷⁵ Lawrence Berkeley National Laboratory, Berkeley, California, United States
- ⁷⁶ Lund University Department of Physics, Division of Particle Physics, Lund, Sweden
- ⁷⁷ Nagasaki Institute of Applied Science, Nagasaki, Japan
- ⁷⁸ Nara Women's University (NWU), Nara, Japan
- ⁷⁹ National and Kapodistrian University of Athens, School of Science, Department of Physics , Athens, Greece
- ⁸⁰ National Centre for Nuclear Research, Warsaw, Poland
- ⁸¹ National Institute of Science Education and Research, Homi Bhabha National Institute, Jatni, India
- ⁸² National Nuclear Research Center, Baku, Azerbaijan
- ⁸³ National Research and Innovation Agency - BRIN, Jakarta, Indonesia
- ⁸⁴ Niels Bohr Institute, University of Copenhagen, Copenhagen, Denmark
- ⁸⁵ Nikhef, National institute for subatomic physics, Amsterdam, Netherlands
- ⁸⁶ Nuclear Physics Group, STFC Daresbury Laboratory, Daresbury, United Kingdom
- ⁸⁷ Nuclear Physics Institute of the Czech Academy of Sciences, Husinec-Řež, Czech Republic

- ⁸⁸ Oak Ridge National Laboratory, Oak Ridge, Tennessee, United States
⁸⁹ Ohio State University, Columbus, Ohio, United States
⁹⁰ Physics department, Faculty of science, University of Zagreb, Zagreb, Croatia
⁹¹ Physics Department, Panjab University, Chandigarh, India
⁹² Physics Department, University of Jammu, Jammu, India
⁹³ Physics Program and International Institute for Sustainability with Knotted Chiral Meta Matter (SKCM2), Hiroshima University, Hiroshima, Japan
⁹⁴ Physikalischs Institut, Eberhard-Karls-Universität Tübingen, Tübingen, Germany
⁹⁵ Physikalischs Institut, Ruprecht-Karls-Universität Heidelberg, Heidelberg, Germany
⁹⁶ Physik Department, Technische Universität München, Munich, Germany
⁹⁷ Politecnico di Bari and Sezione INFN, Bari, Italy
⁹⁸ Research Division and ExtreMe Matter Institute EMMI, GSI Helmholtzzentrum für Schwerionenforschung GmbH, Darmstadt, Germany
⁹⁹ Saga University, Saga, Japan
¹⁰⁰ Saha Institute of Nuclear Physics, Homi Bhabha National Institute, Kolkata, India
¹⁰¹ School of Physics and Astronomy, University of Birmingham, Birmingham, United Kingdom
¹⁰² Sección Física, Departamento de Ciencias, Pontificia Universidad Católica del Perú, Lima, Peru
¹⁰³ Stefan Meyer Institut für Subatomare Physik (SMI), Vienna, Austria
¹⁰⁴ SUBATECH, IMT Atlantique, Nantes Université, CNRS-IN2P3, Nantes, France
¹⁰⁵ Sungkyunkwan University, Suwon City, Republic of Korea
¹⁰⁶ Suranaree University of Technology, Nakhon Ratchasima, Thailand
¹⁰⁷ Technical University of Košice, Košice, Slovak Republic
¹⁰⁸ The Henryk Niewodniczanski Institute of Nuclear Physics, Polish Academy of Sciences, Cracow, Poland
¹⁰⁹ The University of Texas at Austin, Austin, Texas, United States
¹¹⁰ Universidad Autónoma de Sinaloa, Culiacán, Mexico
¹¹¹ Universidade de São Paulo (USP), São Paulo, Brazil
¹¹² Universidade Estadual de Campinas (UNICAMP), Campinas, Brazil
¹¹³ Universidade Federal do ABC, Santo Andre, Brazil
¹¹⁴ Universitatea Nationala de Stiinta si Tehnologie Politehnica Bucuresti, Bucharest, Romania
¹¹⁵ University of Cape Town, Cape Town, South Africa
¹¹⁶ University of Derby, Derby, United Kingdom
¹¹⁷ University of Houston, Houston, Texas, United States
¹¹⁸ University of Jyväskylä, Jyväskylä, Finland
¹¹⁹ University of Kansas, Lawrence, Kansas, United States
¹²⁰ University of Liverpool, Liverpool, United Kingdom
¹²¹ University of Science and Technology of China, Hefei, China
¹²² University of South-Eastern Norway, Kongsberg, Norway
¹²³ University of Tennessee, Knoxville, Tennessee, United States
¹²⁴ University of the Witwatersrand, Johannesburg, South Africa
¹²⁵ University of Tokyo, Tokyo, Japan
¹²⁶ University of Tsukuba, Tsukuba, Japan
¹²⁷ Universität Münster, Institut für Kernphysik, Münster, Germany
¹²⁸ Université Clermont Auvergne, CNRS/IN2P3, LPC, Clermont-Ferrand, France
¹²⁹ Université de Lyon, CNRS/IN2P3, Institut de Physique des 2 Infinis de Lyon, Lyon, France
¹³⁰ Université de Strasbourg, CNRS, IPHC UMR 7178, F-67000 Strasbourg, France, Strasbourg, France
¹³¹ Université Paris-Saclay, Centre d'Etudes de Saclay (CEA), IRFU, Département de Physique Nucléaire (DPhN), Saclay, France
¹³² Université Paris-Saclay, CNRS/IN2P3, IJCLab, Orsay, France
¹³³ Università degli Studi di Foggia, Foggia, Italy
¹³⁴ Università del Piemonte Orientale, Vercelli, Italy
¹³⁵ Università di Brescia, Brescia, Italy
¹³⁶ Variable Energy Cyclotron Centre, Homi Bhabha National Institute, Kolkata, India
¹³⁷ Warsaw University of Technology, Warsaw, Poland
¹³⁸ Wayne State University, Detroit, Michigan, United States
¹³⁹ Yale University, New Haven, Connecticut, United States
¹⁴⁰ Yonsei University, Seoul, Republic of Korea

¹⁴¹ Zentrum für Technologie und Transfer (ZTT), Worms, Germany

¹⁴² Affiliated with an institute covered by a cooperation agreement with CERN

¹⁴³ Affiliated with an international laboratory covered by a cooperation agreement with CERN.